Board-Level Thermal Management Systems with Application in Electronics and Power Electronics

by

Aliakbar Soleymani Koohbanani

B.Sc., Sharif University of Technology, 2013

Thesis Submitted in Partial Fulfillment of the
Requirements for the Degree of
Master of Applied Science

in the
School of Mechatronic Systems Engineering
Faculty of Applied Sciences

SIMON FRASER UNIVERSITY

Summer 2016

Approval

Name:	**Aliakbar Soleymani Koohbanani**
Degree:	**Master of Science**
Title:	**Board-Level Thermal Management Systems with Application in Electronics and Power Electronics**
Examining Committee:	**Chair:** Woo Soo Kim Assistant Professor

Majid Bahrami
Senior Supervisor
Professor

John Jones
Supervisor
Associate Professor

Krishna Vijayaraghavan
Supervisor
Assistant Professor

Date Defended/Approved: March 9, 2016

Abstract

In this study, heat removal and thermal management solutions for electronic devices were investigated at board-level. The generated heat at an electronic chip, installed on a printed circuit board (PCB), can be dissipated either through a heat sink, that is attached directly to the chip, or can be transferred through the PCB to the other side and then be dissipated to the ambient. In any case, thermal interface materials (TIMs) should be used to reduce the thermal contact resistance (TCR) at the solid-solid interface, and also to electrically insulate the live electrical component from the heat sink which is normally exposed to the ambient. Graphite, due to its low cost, lightweight, low thermal expansion coefficient, high temperature tolerance, and high corrosion resistance properties is shown to be a promising candidate to be used as a TIM. In this study, a new analytical model was developed to predict the thermal conductivity of graphite-based TIMs as a function of pressure applied during the production, and flake mechanical properties. The model was verified with the experimental results obtained from testing multiple graphite-based TIM samples.

Transferring the heat to the back of the PCB could potentially provide more surface area for the heat transfer, as normally the backside of PCBs is less populated compared to the front side. However, this comes with its own challenges, due to the low thermal conductivity of the FR4, the main material used in the PCB composition. Thermal vias, which are copper-plated through holes, are proposed as a solution, since they can provide a thermal bridge for heat. A new analytical model was developed for predicting the enhanced thermal conductivity of PCBs equipped with thermal vias. The results were validated by the experimental data obtained from testing nine PCB samples. Effects of vias diameter and their arrangement on the thermal performance were investigated. The results indicated that by using staggered arrangement of thermal vias with larger diameters, the effective thermal conductivity of the PCB can be improved.

Keywords: Thermal Management; Thermal Interface Material (TIM); Printed Circuit Board (PCB); Thermal Via; Graphite-based TIM; Experimental Study; Numerical Simulation

To my beloved family

Acknowledgements

I wish to express my sincere gratitude towards my senior supervisor, Dr. Majid Bahrami for his kind support, encouragement, and expert guidance throughout my graduate studies. Working with Dr. Bahrami was an excellent experience and a great privilege for me.

I am profoundly grateful to Dr. Mehran Ahmadi, whose insightful and brilliant guidance helped me since the beginning of this journey until the very end. I would also like to thank Dr. Mohammad Fakoor Pakdaman and Dr. Mohammad Ali Fayyazbakhsh for their intellectual contributions to my research.

I would like to thank all my friends and colleagues at the *Laboratory for Alternative Energy Conversion* (LAEC) for their kindness and the remarkable atmosphere they created.

I would also like to thank Terrella Energy Systems and especially Dr. John Kenna for the useful comments and support of this research. This research made use of the 4D LABS shared facilities supported by the Canada Foundation for Innovation (CFI), British Columbia Knowledge Development Fund (BCKDF), Western Economic Diversification Canada (WD), and Simon Fraser University (SFU).

Table of Contents

List of Tables

List of Figures

List of Acronyms

ASTM	American Society of Testing and Materials
LED	Light Emitting Diode
NFG	Natural Flake Graphite
TCR	Thermal Contact Resistance
PCB	Printed Circuit Board
PCM	Phase Change Material
PEM	Polymer Electrolyte Membrane
RMS	Root Mean Square
SEM	Scanning Electron Microscope
TIM	Thermal Interface Material

Symbols

General Symbols

a	Gap length between graphite flakes, *m*
A	Area, m^2
c_1,c_2	Vickers micro-hardness coefficients, *GPa*
D	Diameter, *m*
F	Force, *N*
H	Micro-hardness, *GPa*
k	Thermal conductivity, *W/mK*
l	Graphite flake length, *m*
m	Mean absolute surface slope
N	Number of thermal vias
p	Number of flakes in width of graphite sheet
P	Pressure, *Pa*
q	Number if flakes in length of graphite sheet
Q	Heat flux*, W*
R	Thermal resistance, *K/W*
S	Spacing between vias
t	Thickness of test samples, *m*
T	Temperature*, K*
u	Length of straight unit cells, *m*
v	Length of staggered unit cells, *m*
x	Distance, *m*

Greek Symbols

σ	RMS surface roughness of graphite flake, μm
ω	Constriction resistance factor
λ	Graphite flake aspect ratio
δ	Graphite flake thickness, *m*

Subscripts

ave	Average

b	Bottom
eff	Effective
i	Inner
ip	In-plane
o	Outer
s	Sample
t	Top
tp	Through-plane
unit	Unit cell properties
x	Horizontal direction
y	Vertical direction

Executive Summary

The performance of electronic components has been significantly improved in the past few decades. This has led to higher functionality, while they are constantly getting smaller in size. From thermal designers' point of view, it means higher heat dissipation from smaller footprints or in other words, higher power densities. If the generated heat in electronic components is not transferred to the environment properly, it causes the temperature to increase gradually, leading to formation of local hot spots and failure of the device. The rate of failure due to thermal issues is doubled with every 10°C increase in the temperature of electronic devices. In general, about 55% of all the failures in electronic devices occur due to overheating caused by improper thermal management.

In this study, heat removal and thermal management solutions for electronic devices were investigated at the board-level. The generated heat in an electronic chip, installed on a printed circuit board (PCB), can be dissipated through a heat sink that is directly attached to the heat-generating component. Alternatively, the generated heat can also be transferred through the PCB to the other side, which is generally less populated and provides more surface area for heat transfer to the ambient. In any of the above-mentioned scenarios, thermal interface materials (TIM) should be used to electrically insulate the live electronic component from the heat sink side that is normally exposed to the ambient, and to reduce the thermal contact resistance (TCR) between the chip and the heat sink. TCR is usually the dominant resistance against heat transfer in the network of thermal resistances and forms a bottleneck that hinders effective heat removal. The second method, *i.e.*, heat removal from the back side of the PCB, is also associated with complexities, since the through-plane thermal conductivity of PCB is usually low due to the low thermal conductivity of FR4, the main material in the PCB composition. The focus of this study is to enhance the heat conduction through TIM and PCB by identifying and improving the effective parameters in the heat transfer.

Motivation

Remarkable properties of graphite, such as mechanical strength, resistivity against corrosion, lightweight, exceptionally high in-plane thermal conductivity, and reasonable price have made it interesting for different cooling and thermal management applications. Natural flake graphite (NFG) can be compressed to form a graphite sheet to be used as a promising material for manufacturing heat exchangers, heat sinks, and TIMs. In a research collaboration, Dr. Bahrami's *Laboratory for Alternative Energy Conversion (LAEC)* at SFU and *Terrella Energy Systems,* a British Columbia (BC)-based industry partner, developed high performance compressed NFG sheets that can be used as TIMs in order to mitigate the TCR. Terrella Energy Systems is currently manufacturing a variety of graphite sheets with different properties and structures, which can be improved even further to push the limits of thermal management in electronic devices.

The focus of the first part of this study is to analyze the parameters that contribute to the thermal properties of graphite sheets, and to improve their anisotropic thermo-physical properties to enhance the trough-plane thermal conductivity. The second part of this study is focused on improving the through-plane thermal conductivity of the PCB. One of the major challenges facing the current technology of PCBs is to remove the dissipated heat from electronic components effectively to prevent failures caused by overheating and thermal stresses. *LAEC*, in collaboration with *Delta-Q Technologies*, another BC-based industry partner, started investigating PCBs with high through-plane thermal conductivity. The enhanced through-plane thermal conductivity can be achieved through using thermal vias. Thermal vias are through holes with a thin layer of copper plated inside them, which can act as thermal bridges that connect both sides of PCB together and provides a low resistance path for the heat being transferred across the PCB. The arrangement and geometry of thermal vias can be optimized so that it will lead to highest thermal conductivity for the PCB. The focus of the second part of this research is to find the optimum arrangement and geometrical parameter for thermal vias, to maximize the through-plane thermal conductivity of PCBs.

Research Objectives

The objectives of the first part of the research in the area of graphite-based TIMs are:

- Measure the anisotropic thermal conductivity of the developed compressed NFG sheets and identify the parameters that contribute to their thermal performance;
- Understand the geometry of graphite flakes and their orientation inside the graphite sheet; and
- Develop an analytical model that can accurately predict the anisotropic thermal conductivity of the compressed NFG sheets, based on flake properties and compressive pressure.

The objectives of the second part of the research on improving thermal conductivity of PCBs through using thermal vias are:

- Develop an analytical model that can assess the through-plane thermal conductivity of PCBs with different arrangements of thermal vias; and
- Identify the best arrangement and vias' diameter that leads to the highest thermal conductivity of the PCB.

Methodology

In this study, an analytical model was developed for assessing the effect of pressure and flake properties on thermal conductivity of compressed graphite sheets. Several scanning electron microscope (SEM) images were taken from the cross section and plane surface of the compressed graphite sheets to understand the geometry and orientation of graphite flakes inside the sheet. A unit cell, which is representative of the whole structure, was defined and a solution for thermal conductivity of the unit cell was extended to the whole structure for both in-plane and through-plane directions. Unit cell approach was also used for modeling the effect of thermal vias on thermal conductivity of PCBs. Two different unit cells for staggered and straight arrangements were defined and their thermal conductivity was calculated using 1-D thermal analysis.

A custom-made test bed based on ASTM D 5470 standard was used to measure the effective thermal conductivity of graphite sheets and PCB samples. At the end, the analytical model was compared against the experimental results. A roadmap of the project is shown in the figure below.

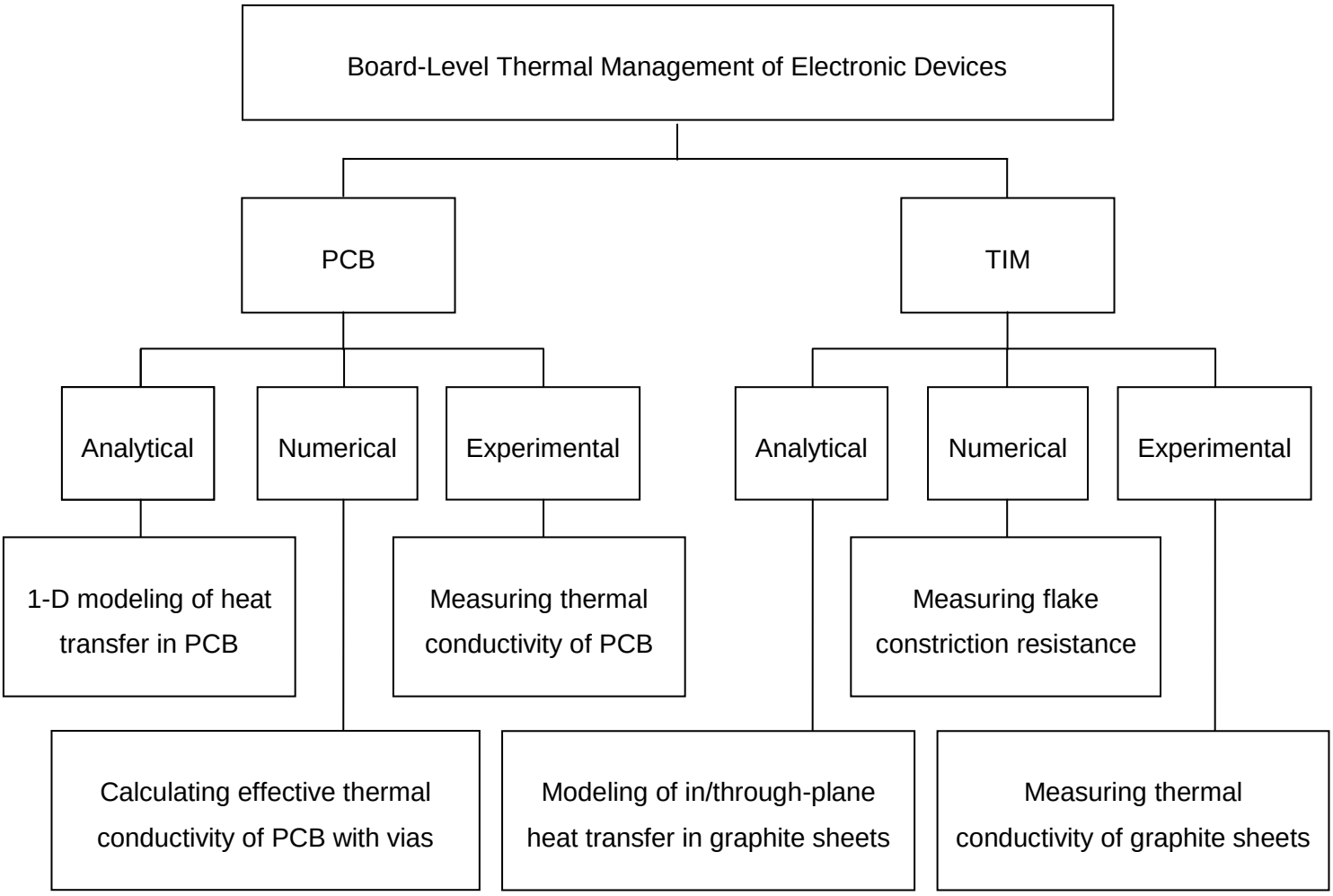

Chapter 1.

Introduction

1.1. Research Importance

The performance of electronic components has significantly improved in the past few decades. This has led to higher functionality, while they are constantly getting smaller in size. From thermal designers' point of view, this means higher heat dissipation from smaller footprints or in other words, higher power densities. If the generated heat in these components is not transferred to the environment properly, it causes the temperature of the electronic component to increase gradually, leading to formation of local hot spots and failure of the device. The rate of failures due to thermal issues doubles with every 10˚C increase in temperature of electronic devices if the operating temperature is above 80˚C [1]. In general, about 55% of all the failures in electronic devices occur due to overheating caused by improper thermal management [2]. Nowadays, thermal management of electronic devices has variety of applications in many industries including aerospace industry, automotive industry (electric vehicles, fuel cell vehicles, hybrid vehicles, and even internal combustion engine vehicles), telecommunication industry (data centers and field enclosures), renewable energy systems (wind turbines and solar panels power electronics), and light emitting diode industry (LED) [3]. Given the fact that the power density of electronics and power electronics has a continuously increasing trend, it is evident that efficient thermal management is essential for durability of electronic devices and has become a limiting factor in the development of the related industries [3–5]. The worldwide market for thermal management is also reflective of its significance. According to BCC research centre, the global market for thermal management of electronic devices was worth $10.1

billion in 2013 and is expected to grow with an annual compound growth rate of 8.4% to reach $14.7 billion by 2019 [6].

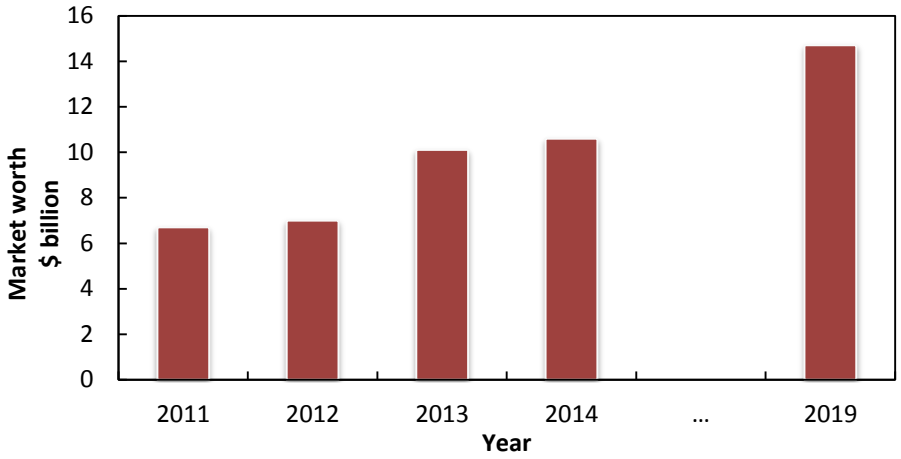

Fig. 1. Expansion of worldwide market for thermal management of the electronics

Around 84% of the worldwide market is related to the hardware products, including fans, heat sinks, heat spreaders, etc. Software products also contribute to the thermal management business and make up 6% of the global market. Thermal interface materials (TIM) are responsible for 6% of the market and the share for substrate is the remaining 4% of the global market [6].

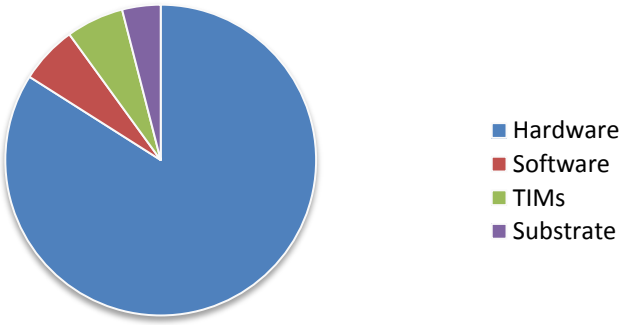

Fig. 2. Global market of the electronics thermal management systems

1.2. Thermal Interface Materials (TIMs)

In order to prevent overheating and maintain the recommended operating temperature in the electronic devices, the generated heat must be dissipated to the surroundings through a complex network of thermal resistances. In most cases, thermal contact resistance (TCR) is present in the network of thermal resistances at any interface between mating surfaces. Since even very smooth surfaces have micro roughness and out of flatness, perfect contact does not occur at the interface and the actual area of contact is limited to only a discrete number of locations where intimate contact occurs [7]. In addition, the contact spots are distributed randomly over the interface, depending upon the properties of both mating surfaces and type of clamping force which is pressing the surfaces together [8]. For a given normal force acting on the interface, the distribution of the contact spots and actual area of contact depend on the surface properties of the mating bodies, including surface roughness, but as a general rule, the actual area of contact is only a few percent of the nominal contact area [9]. Generally, heat can be transferred across the interface by conduction through the actual contact area or by conduction through air, which might be present in the voids at the interface. Since thermal conductivity of air is low, most of the heat would pass through the contact spots.

TCR is the bottleneck in many cooling and thermal management applications. Therefore, in order to design a well-functioning cooling system, proper precautions must be taken to avoid failure. In general, TCR may be mitigated by two methods: (1) increasing the actual contact area that leads to a larger area of the heat transfer. This can be accomplished by increasing the clamping pressure acting on the mating surfaces, or making the surfaces smoother by decreasing their roughness and out-of-flatness, before the joint is formed; and (2) applying a TIM to the joint. When applied at the interface, TIMs tend to conform to the roughness, hills, and valleys of the mating surfaces and fill the gap between them and remove the insulating air. TIMs should have high thermal conductivity to be able to transfer heat across the interface effectively.

Since electronic components and circuit boards as fragile and sensitive to mechanical stress, there are load constraints that make it impossible to exert high clamping pressures, in order to increase the actual contact area and mitigate the TCR. Intel specifies a maximum clamping force of 111.2N can be applied between a P4 processor and its heat sink [10]. On the other hand, manufacturing perfectly smooth surfaces is not feasible with the current technology. Therefore, the only practical solution for mitigating high TCR is to use TIMs at the interface while maintaining a moderate clamping pressure.

Any interstitial substance which is able to fill the gap at interface is capable of reducing TCR if its thermal conductivity is higher than air [11]. However, in order to achieve minimum thermal resistance, TIMs should possess the following properties:

1- High thermal conductivity, which helps transfer heat across the interface effectively;

2- Compliance, or the ability to conform to the contacting surfaces by small contact pressures and filling the gap perfectly;

3- Minimal thickness, to minimize bulk thermal resistance of the TIM itself;

4- Durability, to maintain performance without degradation;

5- Being non-toxic;

6- Manufacturing-friendly, and being easy to apply and remove [12].

There are many different types of TIMs, including greases, adhesives, solders, phase change materials (PCMs) , gels, graphite sheets, etc. [13]. Among different types of TIMs, thermal greases are widely used. Thermal greases are made from a polymer matrix filled with particles, such as alumina, silver, and silica whose thermal conductivity is relatively high. Thermal greases require high volume fractions of particles (50-70 vol. %) to reach thermal conductivity range of 1-5 W/mK [14–16]. Another type of TIMs that is commonly used is PCM. PCMs are usually low temperature thermoplastic adhesives with low melting point in the range of 50-80˚C [17]. Similar to thermal greases, PCMs also have different configurations with fillers, in order to increase their thermal

conductivity. PCMs are generally designed to have a melting point lower than the operating temperature of the electronic device, so that they would melt before critical temperatures are reached. On the other hand, if the melting temperature of the PCM is too low, it would raise the possibility of melting due to high ambient temperatures [18].

The main failure modes in TIMs are pump out, dry out, delamination, cracking, and degradation. Pump out occurs when two contacting surfaces with different coefficients of thermal expansion undergo a temperature cycle, which causes relative movement between the surfaces. This cyclic movement will cause the interstitial material to be squeezed out of the interface. This phenomenon is usually referred to as “pump out” and leads to reduction of thermal grease at the interface which increases TCR [19,20]. Dry out occurs when the polymer matrix is separated from the filler particles at high temperatures. After being separated from particles, the polymer tends to flow out of the interface partially, which results in drying out. In addition to elevated temperatures, high humidity levels can also affect the thermal resistance of thermal greases [21]. In conclusion, despite their excellent ability to fill the gaps at any interface and their satisfactory thermal conductivity, thermal greases are prone to degradation and lose their performance over time. Therefore, a substitute for thermal greases with high performance and durability must be found.

Table 1. Characteristics of the most common TIMs in the market

TIM type	Thermal conductivity (W/m·K)	General Characteristics	Advantages	Disadvantages
Thermal Greases	1-5 [22–24]	Silicone-based matrix loaded with particles to enhance thermal conductivity	High thermal conductivity Low viscosity that enables the material to fill surface asperities	Susceptible to grease pump out and phase separation [20]
PCMs	0.1-3 [25,26]	A substance with a high heat of fusion which is capable of storing and releasing large amounts of energy	Higher viscosity compared to greases leads to increased stability Application and handling is easier compared to greases	Lower thermal conductivity than greases
Graphite-based TIMs	3-10 [28,29]	Layered structure with strong covalent bonds within the layers, and weak Van-der-Waals bonds connecting the layers	Higher thermal conductivity than other types of TIMs Degradation resistivity Application and handling is easier due to increased mechanical strength	Does not fill the surface asperities as effectively as thermal greases

A potential candidate for replacing thermal greases as TIMs could be graphite sheets. Graphite has excellent thermal conductivity, which can be beneficial for heat transfer at interface. Moreover, it is flexible and has the ability to conform to surface roughness and out-of-flatness of any surface to replace the insulating air. In addition, pump out and dry out which are the two major modes of degradation in TIMs, do not occur for graphite sheets. The first section of this study is focused on utilizing compressed natural flake graphite (NFG) sheets as a TIM and investigates the advantages of graphite sheets over commercialized TIMs that are commonly used today.

1.3. Printed Circuit Boards (PCBs)

The significant impact of PCB properties on the operating temperature of different electronic devices has been shown through many studies [30–32]. According to studies available in the literature, between 40 to 96% of heat being generated in an electronic chip could be transferred to PCB [33–36]. The studies confirm that PCB

properties directly affects the operating temperature of electronic components that are installed on it [37].

One of the popular thermal management methods, specifically for highly-populated electrical boards, is to transfer the heat generated in the components to the back-side of the PCB, and then dissipate it to the ambient using heat sinks or other cooling methods. PCBs provide mechanical support and connect components electronically. One of the major challenges facing the current technology of PCB is to remove the dissipated heat from electronic components effectively to prevent failures caused by overheating and thermal stresses. This task can be achieved via attaching a heat sink to the backside of the PCB. PCBs are generally made of several layers of FR4, which is a composite material made of woven fiberglass with epoxy resin binder and has low thermal conductivity. The low through-plane thermal conductivity of FR4; however, is the main drawback of this cooling method. Thus, for this cooling method, in which the PCB may be the bottleneck for the heat flow, a proper design of the PCB is essential [38].

The interconnect network of copper in PCB not only electronically connects the components, but also contributes to the effective thermal conductivity of the PCB. Thus, the effective thermal conductivity of PCB is higher than pure FR4 [39]. PCBs are highly anisotropic, due to their layered structure. Thermal conductivity of PCB in in-plane direction is higher compared to its through-plane direction; however, the through-plane thermal conductivity of PCB is more crucial for thermal management purposes.

In order to increase the thermal conductivity of the PCB, an array of copper plated through holes can be used to transfer heat from one side of the PCB to the other. These copper plated through holes are usually referred to as thermal vias. If thermal vias are located on PCB effectively, the through-plane thermal conductivity of the PCB will be greatly increased which can prevent local hot spots formation and increase the circuit life time [32]. On the other hand, adding thermal vias will increase the cost, weight, and complexity of the PCB design. As a result, it is important to have an in depth

understanding of heat transfer through the thermal vias and their contribution to the effective thermal conductivity of PCB.

Chapter 2.

Graphite-based TIMs

2.1. Preface

Graphite is by far the most important type of carbon and has recently drawn immense attention, due to its interesting properties, such as high thermal conductivity, electrical conductivity, flexibility, degradation resistivity, lightweight, and high mechanical strength. Graphite has different forms that fall under two major categories: natural and synthetic graphite [41]. Natural graphite is described as a mineral found in nature which consists of graphitic carbon [42]. Synthetic graphite, on the other hand, is made by heat treatment and orienting the disordered layers of unstructured carbon into graphitic structure. NFG has exceptional thermal conductivity of 2200 W/mK in its in-plane direction [43]. In-plane thermal conductivity of graphite sheets manufactured by compressing NFGs had been reported to be 350-650 W/mK [44–46]. These properties, especially high thermal conductivity, have made graphite sheets suitable for different cooling and thermal applications, such as heat exchangers, heat spreaders, TIMs and bipolar plates of polymer electrolyte membrane (PEM) fuel cells.

Terrella Energy Systems is one of the companies that are trying to utilize the excellent thermal properties of graphite, in order to manufacture highly functioning heat exchangers, heat spreaders, and TIMs. Terrella specializes in roll embossing technology using flexible NFGs for application in energy and thermal management systems. They have the capability to manufacture products with precise features from highly conductive NFGs at high volumes.

Terrella has developed several types of compressed NFG sheets with different microstructure and properties. Measuring the thermal conductivity of the compressed NFG sheets produced by Terrella was the first step to understand the advantages and drawbacks of their current technology. Comparing the thermal performance of different types of graphite sheets provides an opportunity to understand the factors that govern their thermal conductivity. This understanding helps the researchers to identify the opportunities for improvement in thermal performance of the product. For this purpose, NFG sheets were tested in Dr. Bahrami's Laboratory for Alternative Energy Conversion (LEAC) and their thermal conductivity was measured. In the next sections, the experimental procedure is explained and the results are discussed.

2.2. Literature Review

Graphite has recently drawn immense attention, due to its excellent thermal, electrical, and mechanical properties and there are many studies that discuss the potential applications of graphite-based materials. Smalc et al. [47] assessed the thermal performance of graphite heat spreaders using both numerical and experimental methods. Their results showed that these materials could be greatly beneficial for usage in heat transfer applications. Taira et al. [48] also elaborated on performance improvement of stacked graphite sheets for cooling applications. They showed that replacement of graphite sheets could considerably improve the performance of electronic cooling systems. Graphite-based materials can also be used to manufacture bi polar plates for PEM fuel cells. Hermann et al. [49] studied the application of graphite composites for this purpose and indicated that graphite has several advantages over metals, such as lower contact resistance and higher corrosion resistance.

Mills et al. [50] studied the thermal conductivity enhancement of PCMs using graphite matrices. The thermal conductivity of paraffin wax increased by two orders of magnitude through impregnating porous graphite matrices with the paraffin. Li et al. [51] conducted experimental and numerical studies and examined the effect of expanded graphite on effective thermal conductivity of paraffin. Their results indicated that the

effective thermal conductivity of pure paraffin could be greatly enhanced by 41 times through adding expanded graphite to paraffin. Zhou et al. [52] developed an analytical model to predict the in-plane thermal conductivity of composites with oriented graphite flakes by incorporating interfacial thermal resistance. Their results indicated that larger sizes of graphite flakes lead to higher thermal conductivities. In a separate study, Zhou et al. [53] developed a new analytical model that could predict the in-plane thermal conductivity of NFG/polymer composites. They investigated the effect of adding carbon nanotubes and graphene to the base material. Their results indicated that in-plane thermal conductivity increased by adding carbon nanotubes and graphene to the base material.

The in-plane thermal conductivity of graphite sheets has been well studied and there are many papers in the literature that have analytically modeled and experimentally measured the in-plane thermal conductivity of the graphite sheets [36-38]. The through-plane thermal conductivity of the graphite sheets; however, has not been thoroughly studied yet, even though in some applications, such as TIMs, the through-plane thermal conductivity of the graphite sheets is more important. Bagheri et al. [54] developed an analytical model to study the impact of orthotropic graphite sheets in plate heat exchangers. They proved that in order to achieve highest efficiency, the larger thermal conductivity should be in the through-plane direction.

In this study, a new analytical model for both through-plane and in-plane thermal conductivities of compressed NFG sheets were developed and the contributing factors to thermal conductivity of graphite sheets were investigated. Thermal performance of graphite sheets in general, is a function of manufacturing process and micro structural properties of graphite flakes. Graphite sheets are highly anisotropic and there is a huge difference between their in-plane and through-plane values of thermal conductivity, which is mainly caused by flake orientation. In order to estimate the effective thermal conductivity of graphite sheets, a closer look at the micro and nanostructure of the material is necessary. The structure of a graphite sheet can be considered to be consisted of micro-scale flakes stacked upon each other [55]. Based on this assumption, which considers the average statistical arrangement, a specific arrangement of the

flakes can be identified as a unit cell or a self-consistent field. A unit cell is a representative geometry, which is repeated in the structure and has the same properties and characteristics as the whole structure.

Since graphite flakes are stacked on top of each other, TCR will appear in the network of thermal resistances of the unit cell. Heat can be transferred across the interface between two graphite flakes by three modes: 1) heat conduction through the contact points on the rough surface of the graphite flakes, 2) conduction through the interstitial air at the voids between the mating surfaces and 3) radiation across the interface. Heat transfer due to thermal radiation can be neglected when temperature difference across the interface is not too high [56]. In this study, the interstitial air was considered to be absent, thus limiting the heat transfer across the interface to conduction through the real contact area [57], which is a small fraction of the nominal contact area [58]. Since 1930s, many researchers have aimed at modeling the thermal contact resistance using analytical, numerical, and experimental approaches [59,60]. Development of a general model with high accuracy for predicting TCR is difficult and most of the models published in the literature have their limitations [61,62]. Bahrami et al [63] developed a compact analytical model that can accurately predict TCR of nonconforming rough surfaces. In their study, instead of using probability relationships to model the size and number of microcontacts of Gaussian surfaces, they employed a scale analysis approach. They collected more than 880 experimental data points and compared them to the presented model and observed a good agreement between the analytical model and a wide range of the experimental data in the literature.

2.3. Experimental Study

In general, there are two major methods to measure thermal conductivity of different materials. The first method is transient method, which is based on observing the changes in temperature of a sample being tested over time when the ambient temperature changes instantly. The main drawback of this method is that the heat capacity of the material must be known and if this information is not available, the

measured values for thermal conductivity of the sample are not reliable.

The second method, which is referred to as the steady state method, imposes a fixed and controlled heat flux on the surface of the sample being tested. The temperature of the sample is measured at different locations which indicate the temperature gradient in the sample [64–66]. Thermal conductivity of the sample can be calculated based on its temperature gradient and the imposed heat flux. Despite transient method, the heat capacity of the sample is not necessary for calculating the thermal conductivity; however, the steady state method is more time consuming than the transient methods. The steady state methods are recommended when measuring the thermal conductivity of inhomogeneous and anisotropic materials since an effective thermal conductivity is measured.

For this later class of methods, no additional information is required for the thermal conductivity measurement, as it is based on the final, steady state temperatures measured during the test [67,68]. The bulk-property nature of this later class of methods make it more appropriate, and even the only one acceptable for measuring the thermal conductivity of inhomogeneous and anisotropic materials where an *effective* (bulk) value for the thermal conductivity is needed [69,70].

In this study, the micro-scale arrangement of carbon flakes was examined to develop a model for the macro-scale effective thermal conductivity of graphite sheets. The geometrical parameters, such as flake length, flake thickness, and the gap between the flakes in the unit cell were considered to be important modeling parameters. Surface roughness and mean absolute surface slope of the graphite flakes were measured using atomic force microscopy. The predicted values for the thermal conductivity of the graphite sheets were compared to experimental results and good agreement was observed.

2.3.1. Experimental Apparatus and Principal of Measurement of Through-plane Thermal Conductivity

The through-plane thermal conductivity of all the samples were measured using a guarded heat flux meter machine, which is a custom-made version of ASTM D 5470 standard apparatus. This test bed determines the total thermal resistance of a sample material by measuring the temperature difference across the sample when the heat is passing through it. Metallic cylinder thermocouples with known thermal conductivity were used to measure the temperature and the heat flux and were carefully placed along the heat flux meters. The schematic of the test bed is shown in Fig. 3. The test bed consists of a base plate made of stainless steel, and a bell jar made of glass enclosing the test column. From top to bottom, the test column consists of the loading mechanism, the steel ball, the heater block, the upper heat flux meter, the sample, the lower flux meter, the heat sink (cold plate), and the load cell. The heater block is a flat copper disk where a cartridge heater is placed. The heat dissipation rate of the heater can be manually adjusted.

Refrigerant circulates inside the cold plate, which is a hollow copper cylinder and connected to a chiller that can adjust the temperature of the refrigerant. A 2000lb load cell, installed under the test column, measures the compressive pressure. The load is applied over a load button placed at the center of the load cell. The flux meters are made of a standard electrolyte iron material with known thermal conductivity. To measure temperatures, six type T thermocouples attached to each flux meter at specific locations, as shown in Fig. 3

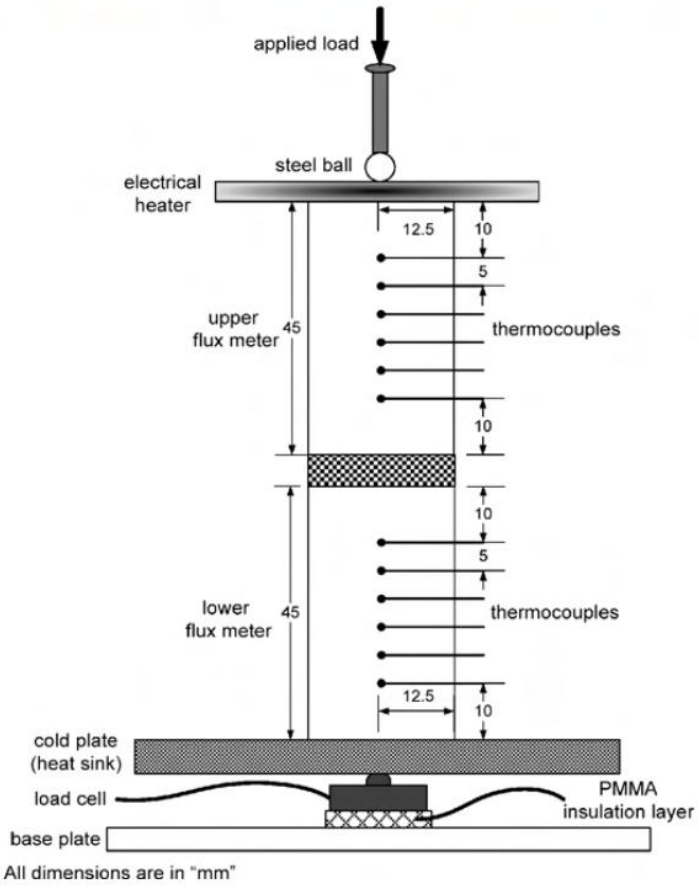

Fig. 3. Schematic of the experimental apparatus used for measuring through-plane thermal resistance of samples

In order to determine the total thermal resistance of the sample, the temperature difference across the sample and the heat flux passing through it need to be calculated. The heat flux passing through the flux meters can be calculated by measuring the temperature gradient across the flux meters using thermocouples, and the temperature difference across the sample can be determined by extrapolating the temperature readings in both flux meters. Using Eq.1, the total thermal resistance can be calculated as:

$$R_{tot} = \frac{\Delta T}{Q} \quad (1)$$

where ΔT is the temperature difference across the sample, Q is the heat flux passing through the sample, and R_{tot} is the total thermal resistance of the sample.

2.3.2. Deriving Through-plane Thermal Conductivity from Total Thermal Resistance (Two-Thickness Method)

It should be noted that the total thermal resistance measured by the guarded heat flux meter device is comprised of two components: the bulk thermal conductivity of the sample itself, and the thermal contact resistance between the sample and the iron heat flux meters. The surface properties of both flux meters and surfaces of the samples are similar, thus the TCR of the interfaces are the same. Therefore, the following equation can be derived:

$$R_{tot} = \frac{t}{kA} + 2 \times TCR \quad (2)$$

where t and k represent the thickness and the through-plane thermal conductivity of the sample, A stands for the cross sectional area of flux meters, and TCR is the contact resistance between the sample and flux meters.

The experiments were conducted on samples prepared with the same manufacturing process. This means they have similar porosity and microstructure. Having the same microstructure implies that the thermal conductivity of the samples are similar, and they have the same surface properties which translates into having the same TCR when they are in intimate contact with flux meters.

If the experiments are run on samples with similar thermal conductivities but with different thicknesses, the bulk thermal resistance of the samples can be separated from the TCR. Given the fact that TCR is independent from thickness [71–75], the through-

plane thermal conductivity of the samples can be calculated using the following equation.

$$k_{tp} = \frac{|t_2 - t_1|}{A\,|R_{tot,2} - R_{tot,1}|} \quad (3)$$

where t_1 and t_2 are the thicknesses of two samples with similar microstructure and different thicknesses, $R_{tot,1}$ and $R_{tot,2}$ are the total thermal resistances of the samples, and A is the area of heat transfer.

2.3.3. Calibration of the Guarded Heat Flux Meter

The guarded heat flux meter machine was used for measuring the thermal conductivity of Pyrex 7740, in order to calibrate the device. Samples of Pyrex with different thicknesses were used for the measurement as explained earlier. The thermal conductivity values for Pyrex were derived and compared to the reported values. The relative difference between the experimental results and the reported data was less than 5%, which has the same order of magnitude as the uncertainty of the guarded heat flux meter device.

2.3.4. Results of Experiments

Terrella Energy Systems has developed five different types of graphite sheets that can be used as thermal interface materials, including compressed NFG sheets, compressed graphite flakes bound with resin, compressed blended graphite flakes, compressed blended graphite flakes with button shape pattern on the surface, and compressed blended graphite flakes bound with resin with button shape pattern and a thin layer of electrical insulation.

These types of graphite sheets were available with different thicknesses from 230-1220 μm, which allows us to use the guarded heat flux meter device in order to measure their through-plane thermal conductivity. The samples could also be cut in

order to prepare different lengths of the same material so that they can be tested in the custom-made in-plane thermal resistance measurement test bed.

The results of through-plane and in-plane thermal resistance measurements are discussed here:

Through-plane Thermal Resistance

Compressed NFG Sheets without Resin

This type of graphite sheet is manufactured by compressing NFGs in order to form a sheet. The manufacturing process results in mostly horizontal orientation for the graphite flakes inside the sheet. Given the fact that the graphite flakes have higher thermal conductivity in the direction of their plane [76,77], the in-plane thermal conductivity of the compressed NFG sheets is expected to be higher than their through-plane thermal conductivity.

There is no resin involved in the production of these graphite sheets, thus it is expected to see some air gaps between the neighbouring graphite flakes. The air that is trapped inside these graphite sheets acts as insulation and lowers the overall thermal conductivity of these graphite sheets.

Four different thicknesses of compressed NFG sheets were tested in the guarded heat flux meter. The names and specifications of these samples are listed in Table 2.

Table 2. Sample names and specifications of compressed non-resin graphite sheets

Sample Name	Thickness (μm)	Type
10-455-01b	1180	Non-resin, Flakes parallel to the plane of graphite sheet
10-455-02b	720	Non-resin, Flakes parallel to the plane of graphite sheet
10-455-03b	500	Non-resin, Flakes parallel to the plane of graphite sheet
10-455-04b	1220	Non-resin, Flakes parallel to the plane of graphite sheet

The samples listed in Table 2 are tested and the results for the through-plane thermal resistance of each sample are depicted in Fig. 4.

Fig. 4 shows that the total thermal resistance of all samples decreases as the compressive pressure is increased. There can be two potential reasons for this. As discussed before, TCR is dependent on pressure and as the pressure increases, the contact resistance between the samples and the flux meters is reduced. As a result, the total thermal resistance of the sample, which is the sum of bulk thermal resistance and the TCR between the sample and flux meters decreases. Another hypothesis is that the compressing force presses the graphite flakes together, thus reducing the void between the flakes by removing the insulating air at the gaps. Removing the air from the gaps in the graphite sheet will lead to higher effective thermal conductivity and will reduce the total thermal resistance of the graphite sheet.

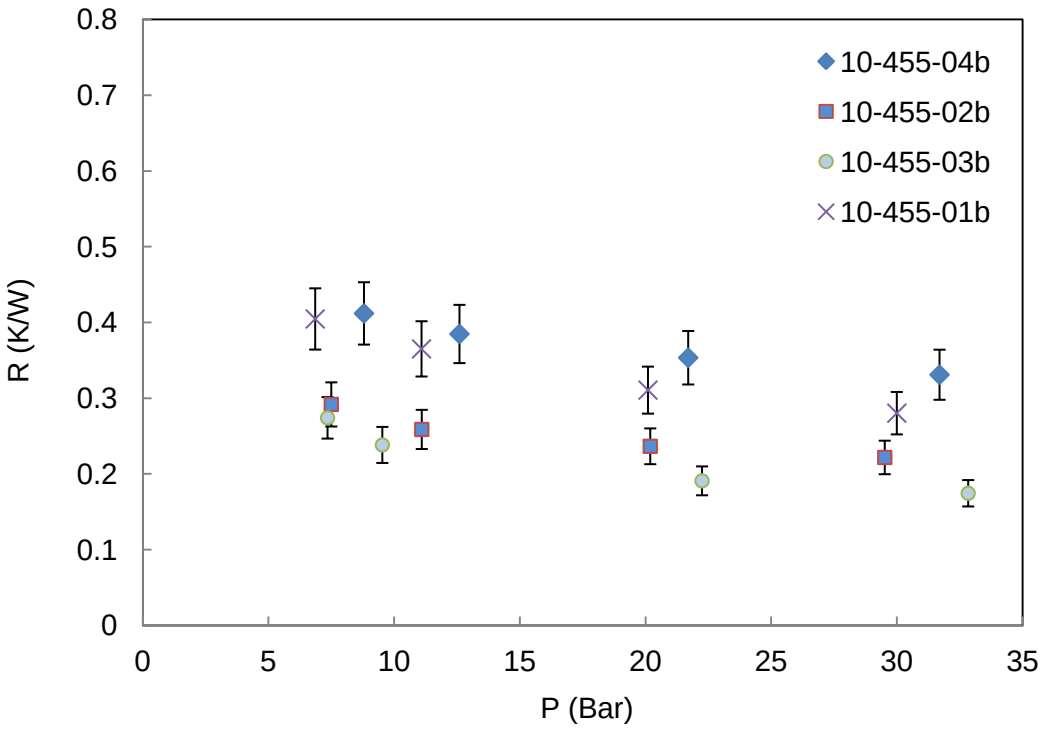

Fig. 4. **Total thermal resistance of compressed graphite flakes without resin**

It is inferred from Fig. 4 that the thermal resistance of thicker compressed non-resin graphite sheets is higher than that of thinner graphite sheets. This is directly related to Fourier's law of conduction, which states that the thermal resistance of any object is directly related to its thickness and inversely related to its thermal conductivity.

Using the two-thickness method between the samples with the highest difference in thickness, the through-plane thermal conductivity of these samples could be calculated. According to ASTM D 5470 standard, the thermal conductivity is measured under 3MPa of compression.

Compressed NFG Sheets Bound with Resin

This type of graphite sheets is very similar to the previous type, in terms of flake orientation, since the manufacturing process is the same; however, they are impregnated with resin that binds the graphite flakes together and forms a strong structure. The first advantage of these types of graphite sheets over the non-resin type is their good mechanical strength. Also, since the graphite flakes are bound together with resin, there should be less insulating air at the gaps between the flakes as it is mostly replaced by resin.

Four different thicknesses of compressed graphite flakes with resin were provided by the supplier and tested in the guarded heat flux meter. The samples names, thickness, and specifications are listed in Table 3. Samples will be identified using their names.

Table 3. Sample names and specifications of the compressed resin containing graphite sheets

Sample Name	Thickness (μm)	Type
10-455-01a	1180	Bound with resin, Flakes parallel to the plane of the sheet
10-455-02a	500	Bound with resin, Flakes parallel to the plane of the sheet
10-455-03a	720	Bound with resin, Flakes parallel to the plane of the sheet
10-455-04a	1220	Bound with resin, Flakes parallel to the plane of the sheet

As mentioned before, most of the flakes in this type of graphite sheets are placed parallel to the plane of the graphite sheet; therefore, the in-plane thermal conductivity of these samples is expected to be higher than the through-plane thermal conductivity. The experimental results for total through-plane thermal resistance of these graphite sheets are shown in Fig. 5.

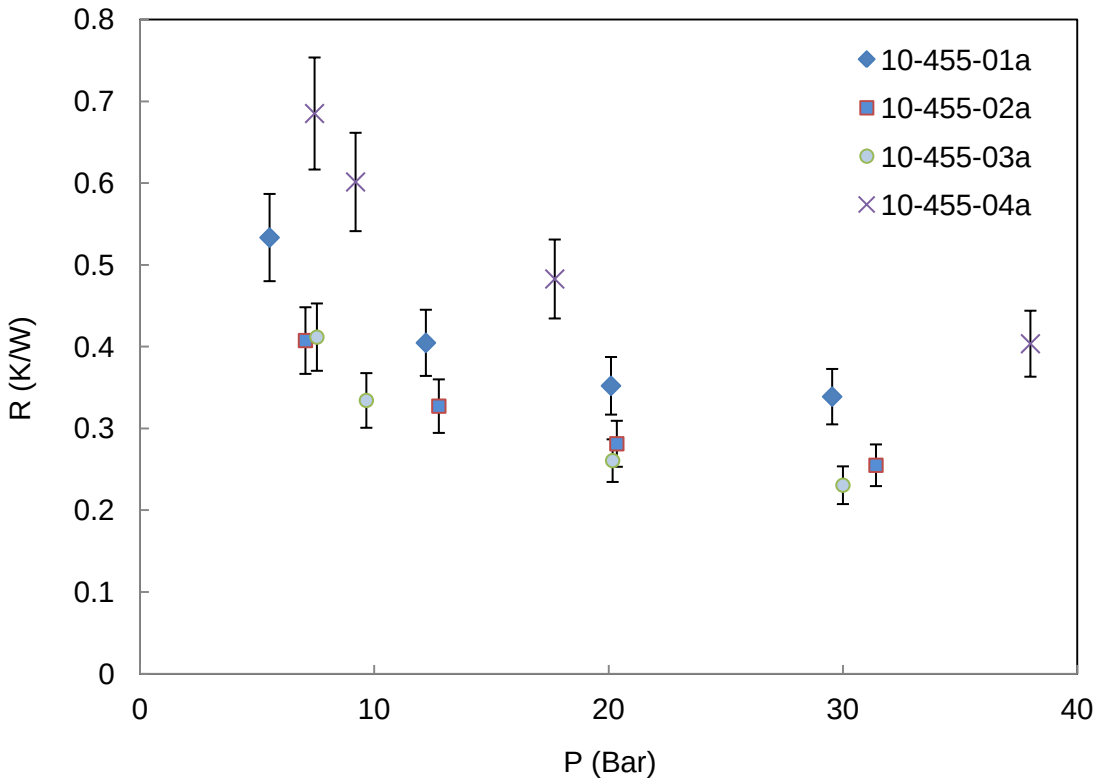

Fig. 5. Total thermal resistance of compressed graphite flakes with resin

From the above diagram, it is clear that the total thermal resistance increases with increasing the thickness, due to escalation of thermal bulk resistance. By comparing Fig. 4 and Fig. 5, it can be inferred that the resin-free graphite sheets exhibit lower thermal resistances, which is contrary to our expectations. The most probable explanation is that when the resin is drawn into the graphite sheets, a thin layer of the resin would remain on the surface of the graphite sheet. This thin film increases the thermal contact resistance between the sample and the flux meters of the test bed. The

formation of this thin layer and the escalation of the value of the thermal contact resistance can also explain why the curves in Fig. 5 corresponding to resin-containing samples are much steeper than those in Fig. 4 that are corresponds to resin-free samples.

Compressed Blended Graphite Flakes

The manufacturing process for the blended graphite sheets are different from the previous types discussed thus far. The difference is that the NFGs are first crumpled and then compressed together. Thus, the graphite flakes are no longer flat. When the crumpled flakes are compressed in the graphite sheet, they have random orientation and despite the compressed resin containing and non-resin graphite sheets, the graphite flakes are no longer placed parallel to the plane of the graphite sheet. Therefore, higher through-plane thermal conductivity is expected for these samples. Accordingly, the in-plane thermal conductivity is expected to be reduced. If the blending procedure is optimally performed, the through-plane and the in-plane thermal conductivities of these graphite sheets should be the same since the flakes are randomly distributed in the graphite sheet. Table 44 shows the names and specifications of these graphite sheets.

Table 4. Sample names and specifications of compressed blended graphite sheets

Sample Name	Thickness (μm)	Type
10-455B-1	230	Non-resin, Blended Graphite flakes
10-455B-2	500	Non-resin, Blended Graphite flakes
10-455B-3	720	Non-resin, Blended Graphite flakes
10-455B-4	1180	Non-resin, Blended Graphite flakes

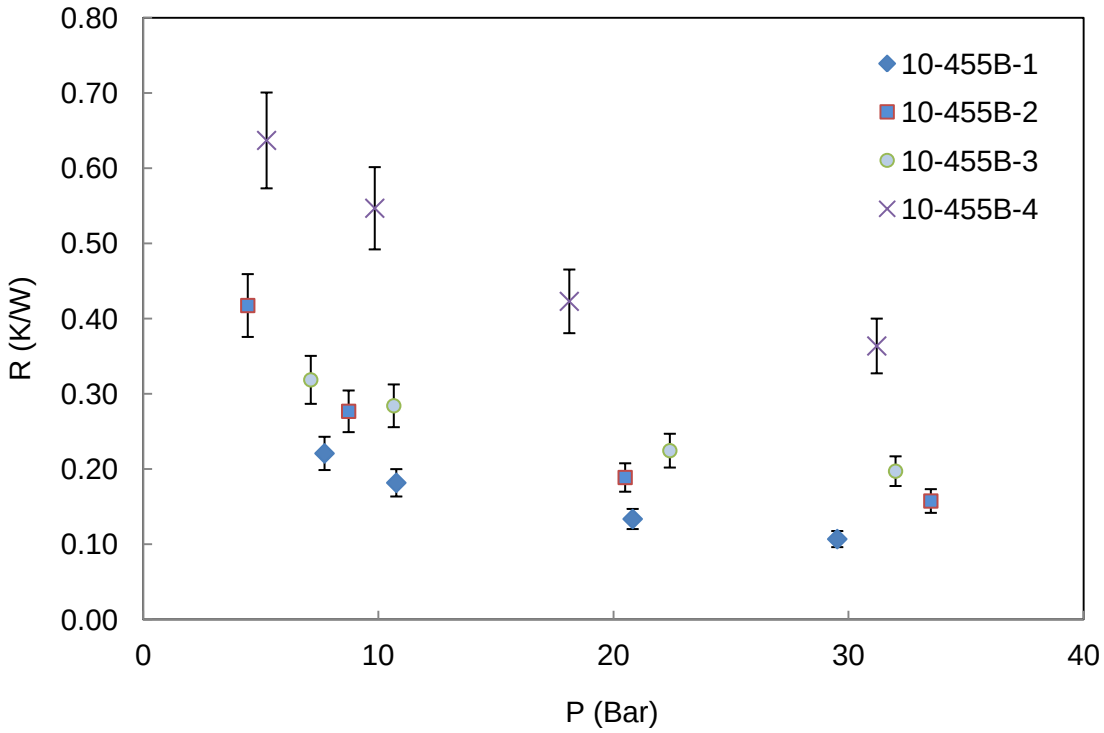

Fig. 6. **Total through-plane thermal resistance of compressed blended graphite flakes**

By comparing the thermal resistances of blended samples with resin-containing and resin-free samples, it can be concluded that the thermal conductivity of the blended samples has been improved due to a different flake orientation in the graphite sheets. This conclusion is based on the assumption that the thermal contact resistance between different types of graphite sheets and the flux meters are the same, since TCR is only dependent on the surface properties of the mating surfaces.

Compressed Blended Graphite Flakes with Patterned Surface

This type of graphite sheets is similar to the compressed blended graphite sheets in terms of flake orientation inside the graphite sheet, which means that flakes tend to have random directions in the graphite sheet. The only difference is the patterned surface, which is implanted on the graphite sheet in an effort to increase the number of graphite flakes that are placed along the through-plane direction, so that the thermal

conductivity of these samples would surpass thermal conductivities of other forms of graphite sheets provided before. On the other hand, higher TCR would be inevitable, as the button-shaped pattern on the surface would impede an intimate contact between the surface of the sample under test and flux meters.

Table 5. Sample names and specifications of graphite sheets with patterned surface

Sample Name	Thickness (μm)	Type
465A-P	230	Non-resin, Blended Graphite flakes, Patterned surface
465B-P	400	Non-resin, Blended Graphite flakes, Patterned surface
465C-P	900	Non-resin, Blended Graphite flakes, Patterned surface
465F-P	400	Non-resin, Flat Graphite flakes, Patterned surface

The patterned graphite sheet 465F-P is different from the rest in terms of flake orientation. Despite the other three, 465F-P is not made of compressed blended graphite flakes and all the flakes in this graphite sheet are placed along its plane. Thus, the through-plane thermal resistance of this graphite sheet is expected to be higher than the rest of graphite sheets in this group. The results for total thermal resistance of all the samples with patterned surface are shown in Fig. 7.

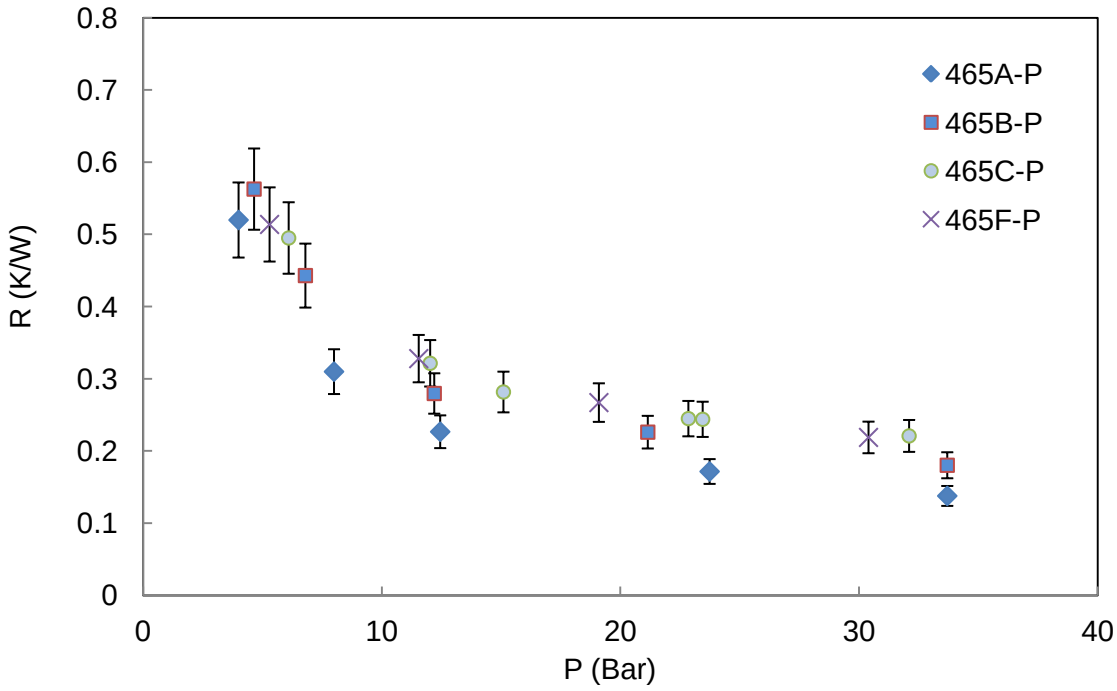

Fig. 7. Total thermal resistance of graphite sheets with patterned surface

As expected, the TCR of these graphite sheets with patterned surface is high compared to that of the compressed blended graphite sheets. This conclusion is based on the significant drop in thermal resistance of the samples. It is noteworthy to mention that the thermal resistance of 465C-P and 465F-P is almost the same, while the thicknesses of these graphite sheets are 0.9 mm and 0.4 mm, respectively. In order to explain this, we need to look at the microstructure of these graphite sheets once more. 465F-P is a button sample with horizontal flakes, while 465C-P is a blended button sample. The blended structure of 465C-P would increase the through-plane thermal conductivity in a way that even though its thickness is more than two times bigger than the thickness of 465F-P, its total thermal resistance is equal to that of 465F-P.

Compressed blended graphite flakes with patterned surface have a lower resistance in comparison to resin containing and non-resin containing graphite sheets, but because of the surface pattern that contributes to contact resistance, thermal

resistance of graphite sheets with patterned surface is larger than those of blended samples.

Compressed Blended Graphite Flakes with Patterned and Coated Surface

In many cases, such as thermal interface materials with applications in power electronics, the electrical conductivity of the TIM must be as low as possible. For this reason, Terrella Energy Systems has developed and manufactured compressed blended graphite sheets with a thin layer of electrical insulation. These graphite sheets are produced with three different coating thicknesses, which results in different breakdown voltages; by increasing the coating thickness, the breakdown voltage would be increased. However, due to the low thermal conductivity of the electrical insulation, an increase in the thickness of the coating would result in lower thermal conductivity. Thus, there is a trade-off between the thermal conductivity, the breakdown voltage of these graphite sheets, and the different coating thicknesses that can be manufactured for different applications, all depending upon the desired thermal and electrical properties. In Fig. 8, the thermal resistances of coated samples with coating thickness of 150 μm are depicted. The thickness of the sample and the coating were used as means of identification.

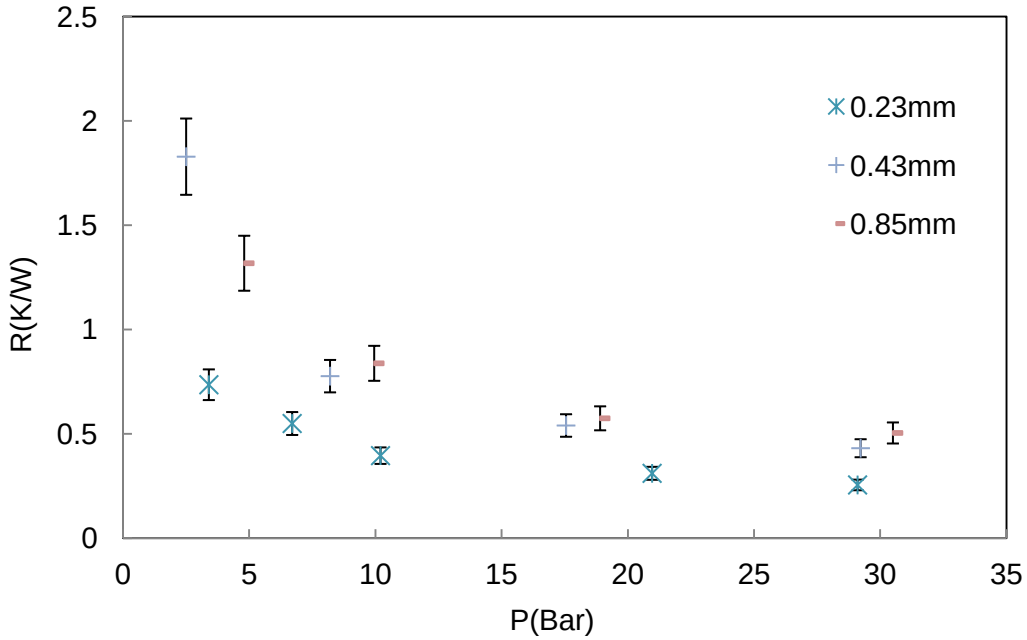

Fig. 8. **Thermal resistance of graphite sheets with 1.5 µm of coating thickness**

Fig. 9 and Fig. 10 show the thermal resistance of coated samples with 2 µm and 3 µm of coating thicknesses, respectively.

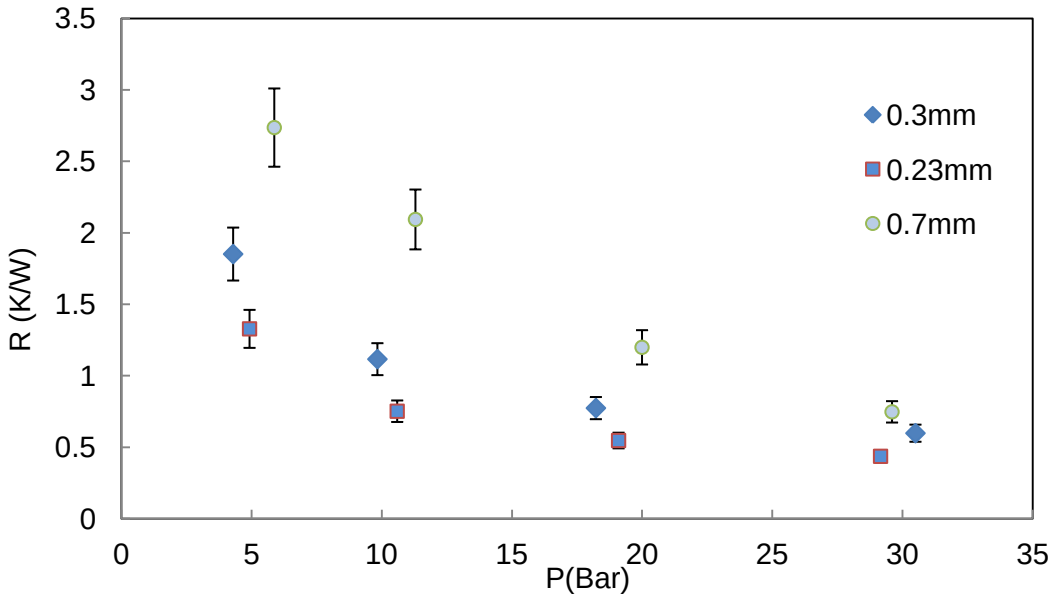

Fig. 9. **Thermal resistance of graphite sheets with 2 µm of coating thickness**

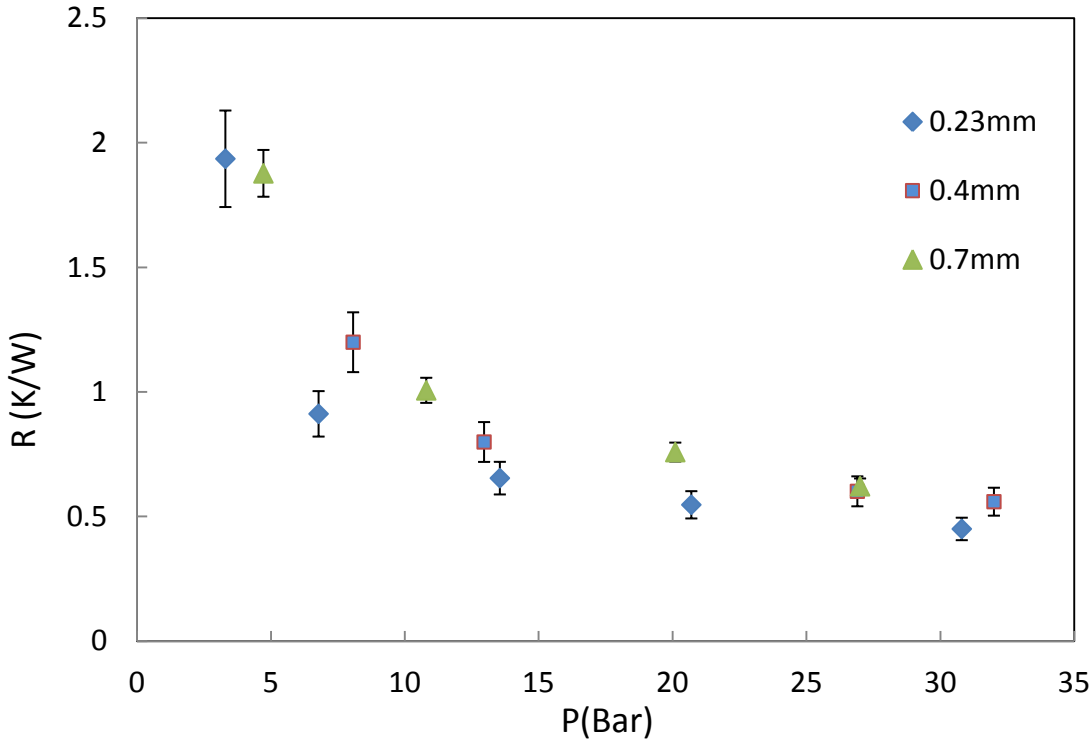

Fig. 10. Thermal resistance of graphite sheets with 3μm of coating thickness

As discussed before, the thermal resistance of graphite sheets significantly increases when the coating thickness is increased. In order to see the effect of coating thickness on the thermal resistance of graphite sheets, the thermal resistance of graphite sheets with the same overall thickness but different coating thicknesses is shown in Fig. 11.

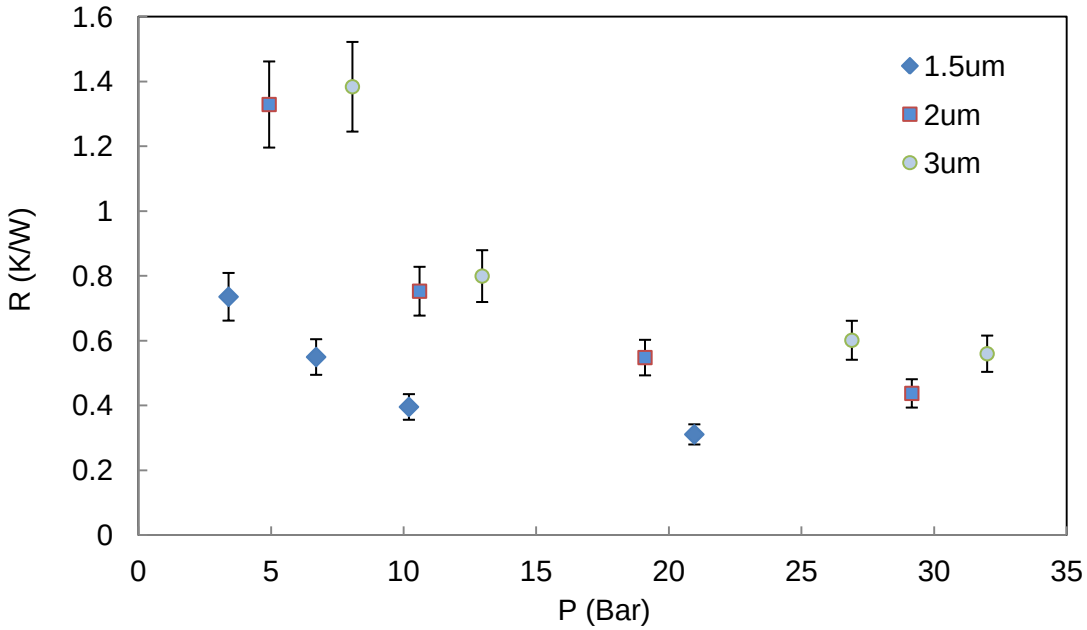

Fig. 11. **Samples with overall thickness of 0.23 mm and different coating thicknesses**

2.3.5. Necessity for an Analytical Model

The experimental study on different types of graphite sheets helped to achieve better understanding of the factors that govern the thermal performance of a compressed NFG sheet. However, an analytical model is required to assess the impact of each factor on the thermal performance and to predict the anisotropic thermal conductivity of the graphite sheets based on the manufacturing process. In the following sections, the past studies in this area will be reviewed, the structure of graphite sheets will be further studied, and an analytical model will be developed.

2.4. Model Development

2.4.1. Geometrical Modeling

In order to develop a model for thermal conductivity of graphite sheets, understanding the geometry and arrangement of flakes inside the graphite sheet is necessary. A promising approach towards understanding the flake size, geometry, and the way they are placed in a graphite sheet is to take several images from their microstructure using scanning electron microscopes (SEM).

Sample Preparation for SEM

In order to take SEM images, which clearly show the structure of graphite sheets and placement of graphite flakes, samples should be carefully prepared for imaging process. This means samples should be cut carefully with a method that leads to minimum distortion in the graphite flakes so that the structure is intact and representative of the graphite sheet. A few methods for preparing samples were attempted and the results are discussed here.

Breaking the Graphite Sheets at Room Temperature

For SEM imaging of the graphite sheet cross-section, the simplest method to prepare the samples is to break the sheet by bending it. Fig. 12 shows a SEM image of the cross section of a piece of graphite sheet that has been broken at room temperature by bending the graphite sheet.

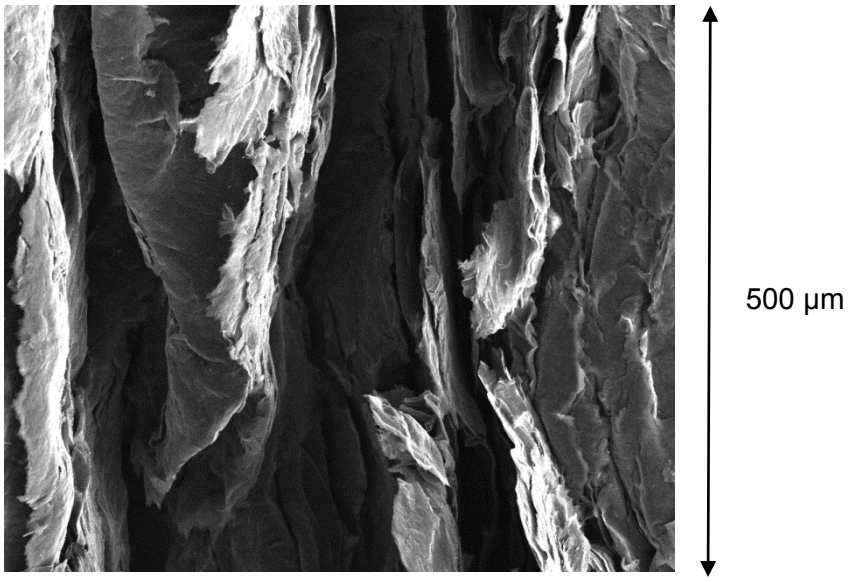

Fig. 12. Cross section of a broken piece of graphite sheet

As Fig. 12 indicates, breaking the graphite sheet leads to some distortion in graphite flakes, thus the structure could not be studied based on these images.

Cutting the Graphite Sheets Using Scissors

Using a scissor to cut graphite sheets is another approach for sample preparation. Several SEM images were taken from small pieces of graphite sheets that were cut with a scissor, as shown in Fig. 13.

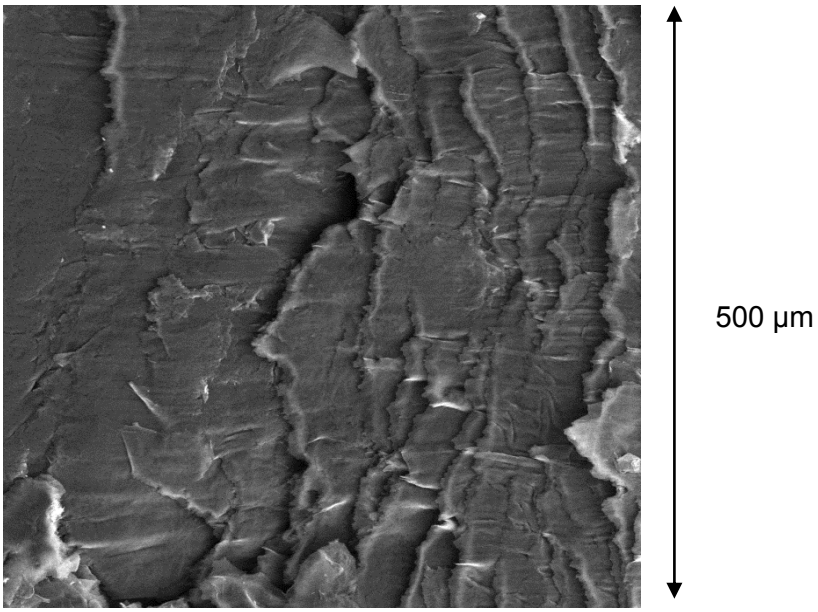

Fig. 13. Cross section of a graphite sheet sample, cut by scissors

Fig. 13 shows that cutting graphite sheets with scissors would lead to deformation in graphite flakes, and the same as breaking, cutting the graphite flakes with scissors will not lead to clear SEM images of the microstructure.

Cutting Graphite Sheets with Sharp Razors

Using sharp razors could help and mitigate the deformation of graphite flakes that happens when scissors are used for sample preparation since they are sharper and thinner than scissors. Therefore, several samples of graphite sheets were cut using razors and the SEM image of their cross section is shown in Fig. 14.

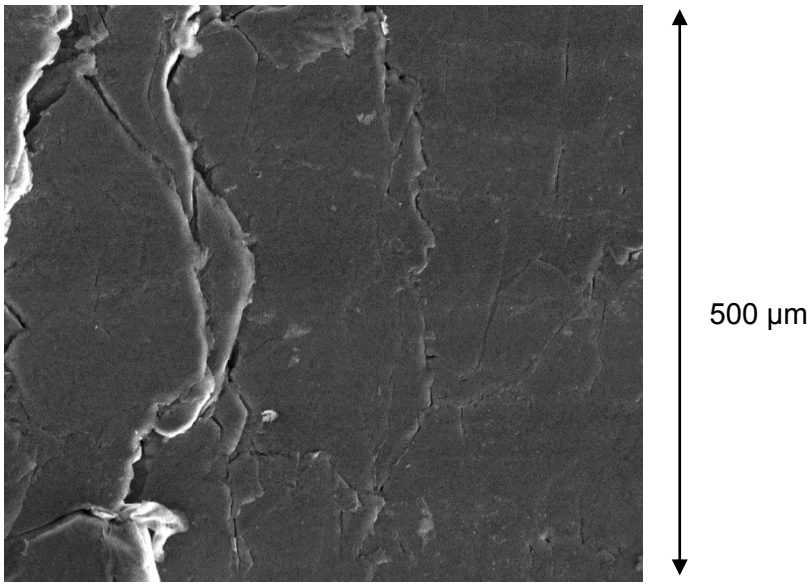

Fig. 14. Cross section of graphite sheet sample cut by sharp razor

Fig. 14 indicates that even using very sharp razors could not prevent distortion in graphite flakes and the SEM images taken from the cross section of the graphite sheets cut with razors does not clearly show the microstructure of the graphite sheets.

Cryogenic Fracture in Graphite Sheets

Cutting the graphite sheets with different methods at room temperature resulted in distortion of graphite flakes. Note that there is resin in a certain type of graphite sheet that could be hardened at cryogenic temperatures. Hardening the resin could add to the mechanical strength of the graphite sheets and reduce the distortion in graphite flakes. Thus, several samples of graphite sheets were prepared by immersing into liquid nitrogen and then breaking them. Fig. 15 shows a SEM image of the cross section of the graphite sheet sample that was prepared using this method.

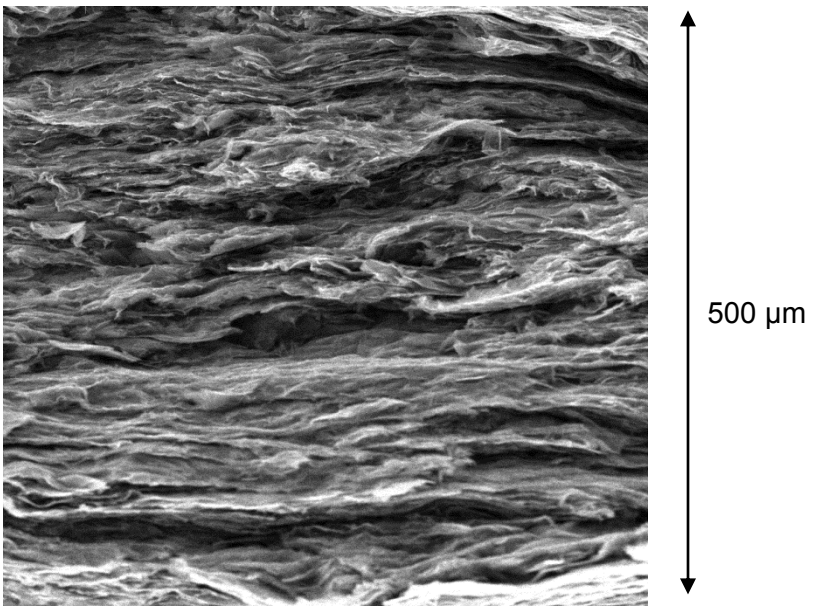

Fig. 15. Arrangement of graphite flakes in a compressed graphite sheet

Fig. 15 shows that there is less distortion in graphite flakes and the microstructure of graphite sheets is clear in this image. Based on the SEM images of the graphite sheets, it is inferred that most of the flakes are aligned in the direction of the plane of graphite sheet.

In order to analytically model the properties of the graphite sheet, the actual geometry of the flakes must be modeled with a simplified schematic. The arrangement of carbon flakes in a piece of graphite sheet is assumed to be a two dimensional structure as shown schematically in Fig. 16. This two-dimensional arrangement is a representative of the actual graphite microstructure. The real flakes, however, are randomly distributed in the micro level and average parameters of the arrangement are taken into account in this model. The values of flake length (L), flake thickness (δ), and gap distance (a) identify the arrangement.

Using this approach, a unit cell was defined within the structure shown by the dashed rectangle in Fig. 16. It is intuitively evident that the entire structure can be mathematically regenerated by arranging consecutively mirrored copies of the unit cell,

and it will be repeated in the entire structure. Thus, a solution of the effective thermal conductivity in the unit cell can be extended to the structure.

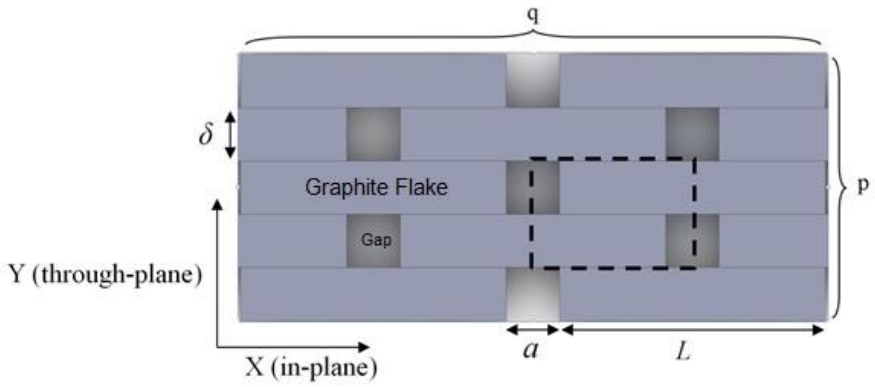

Fig. 16. Schematic of the arrangement of graphite flakes and through-plane unit cell

The objective here is to find the thermal resistance of the proposed unit cell. Having the resistance of the unit cell in the in-plane (horizontal) and through-plane (vertical) directions, the total effective resistance of the whole graphite sheet with unit length and height will be

$$R_{y,eff} = R_{y,unit}\frac{p}{q} \tag{4}$$

$$R_{x,eff} = R_{x,unit}\frac{q}{p} \tag{5}$$

where $Ry,unit$ and $Rx,unit$ are the in-plane and through-plane resistances of the unit cell, respectively, and *p* and *q* are the number of flakes in y and x directions respectively. Ry, and $Rx,unit$ are the effective 500 μm sheet resistances per unit length and height. It is noteworthy that the average flake length is much greater than its thickness (usually 10 times larger) which implies that the number of graphite flakes in the through-plane direction is much more than the number of flakes in the in-plane direction. Therefore, the through-plane resistance of the sheet is expected to be orders of magnitude higher than the in-plane resistance, due to contact resistance between layers.

This has been verified by experiments. The total thermal resistance of the unit cell is comprised of three components: (1) Thermal bulk resistance of each flake, (2) TCR between the adjoining flakes, and (3) constriction resistance within flakes.

$$R_{x,eff} = R_{x,constriction} + R_{x,contact} + R_{x,bulk} \quad (6)$$

$$R_{y,eff} = R_{y,constriction} + R_{y,contact} + R_{y,bulk} \quad (7)$$

2.4.2. Analytical Modeling

One of the most outstanding characteristics of the graphite flakes is their high thermal conductivity [78]. There are many studies in the literature that have focused on measuring the high thermal conductivity of the graphite flakes, and reported values that are higher than 1000 W/m·K [78–81]. Considering the high thermal conductivity of the graphite flakes, the bulk thermal resistance of these materials is not significant and can be neglected.

Constriction resistance can be defined as the resistance introduced to the heat path, due to the changes in cross section area of the heat transfer path. If the geometry of the self-consistent field consisted of only a strip of pure carbon material, then the flake-level constriction resistance will be zero. The small gap between adjoining flakes introduces a constriction resistance. Since the flake aspect ratio (λ) for the graphite flakes used in this study is a large number (20-25), the temperature distribution is almost one-dimensional in most of the self-consistent fields for both the in-plane and through-plane heat transfer cases. Thus, heat transfer only occurs in one dimension and the constriction resistance could also be neglected. Therefore, the total resistance of the graphite sheet is the sum of all the TCRs between the mating graphite flakes.

As explained before, the main thermal resistance in most cases is the TCR. Heat can be transferred across the interface of the two graphite flakes by three modes: 1) conduction through the contact points, 2) conduction through the interstitial air at the

voids between the mating surfaces, and 3) radiation across the air gap between the adjoining surfaces. In this study, the interstitial air was considered to be absent, thus limiting the heat transfer across the interface to the conduction through the contact points [57], which is a small fraction of the nominal contact area [58]. Since 1930s, many researchers have aimed at modeling the thermal contact resistance using analytical, numerical, and experimental approaches [59,60]. Due to the geometry and physics complicacies, development of a general model with high accuracy for predicting TCR is difficult and most of the models published in the literature have their limitations [61,62]. Bahrami et al [82] developed a compact analytical model that can accurately predict TCR of nonconforming rough surfaces. They collected more than 880 experimental data points, compared them to the presented model, and observed good agreement between the developed model and a vast range of the experimental data available in the literature. The following is a summary of the model developed in [82]:

$$R_{contact} = \frac{0.565\, c_1 H^{c_2} (\sigma/m)}{k_s \cdot P \cdot A} \tag{8}$$

where

$$k_s = \frac{2k_1 k_2}{(k_1 + k_2)} \tag{9}$$

k_1 and k_2 are the thermal conductivities of the two mating surfaces, respectively; and

$$\sigma = \sqrt{\sigma_1^2 + \sigma_2^2}, \qquad m = \sqrt{m_1^2 + m_2^2} \tag{10}$$

σ is the surface roughness and m is the mean surface slope of the mating surfaces. Subscripts 1 and 2 refer to the mating surfaces.

To model the through-plane thermal conductivity of the graphite sheets, the heat conduction in through-plane direction in the self-consistent field was considered. Given the fact that both surfaces are made of the same material, Eq. 8 can be written as:

$$R_{y,\,unit} = R_{contact} = \frac{0.565\ c_1 H^{c_2}(^{\sigma}/_{m})}{k \cdot P \cdot A} \tag{11}$$

Thus, the overall through-plane thermal resistance can be calculated by:

$$R_{y,\,eff} = \frac{0.565\ c_1 H^{c_2}(^{\sigma}/_{m})}{k \cdot P \cdot A} \cdot \frac{L}{\delta} \tag{12}$$

Since the resistance was defined for unit dimensions, the effective thermal conductivity can be found as the inverse of the resistance:

$$k_y = \frac{(L-a)\delta}{L}\left(\frac{\omega_y \cdot k \cdot P}{0.565\ c_1 H^{c_2}(^{\sigma}/_{m})}\right) \tag{13}$$

where ω_y is the fitting parameter for the through-plane direction, and is a constant number (its value is given in Table 8).

To calculate the in-plane thermal conductivity of the graphite sheets, these parameters were calculated for the self-consistent field. The overall thermal resistance in the plane of the graphite flakes for the self-consistent field can be written as:

$$R_{x,\,unit} = \frac{0.565\ c_1 H^{c_2}(^{\sigma}/_{m})}{k \cdot P \cdot A} \tag{14}$$

Thus, the overall in-plane thermal resistance of the graphite sheet can be calculated by:

$$R_{x,\,eff} = \frac{0.565\, c_1 H^{c_2}(\sigma/m)}{k \cdot P \cdot A}\frac{L}{\delta} \tag{15}$$

Since the resistance was defined for unit dimensions, the effective in-plane thermal conductivity can be found as the inverse of the resistance:

$$k_x = \frac{L(L-a)}{\delta}\left(\frac{\omega_x \cdot k \cdot P}{0.565\, c_1 H^{c_2}\left(\frac{\sigma}{m}\right)}\right) \tag{16}$$

where ω_x is the fitting parameter for the through-plane direction, and is a constant number (its value is given in Table 8).

2.4.3. Material Characterization

In order to use the aforementioned equations to predict the thermal conductivity of graphite sheets, the dimensions of individual graphite flakes must be known. To accomplish this, several SEM images were taken from graphite flakes and average values for length and thickness of the graphite flakes were calculated and implemented in the model, as shown in

Fig. 17 and Fig. 18. It is observed from these figures that the dimensions of graphite flakes vary and an average value must be implemented in the model.

Table 6. Length and thickness of the graphite flakes

Dimension	Average (μm)	Standard Deviation (μm)
Length	612.1	71.2
Thickness	24.4	12.6
Gap	50	25.3

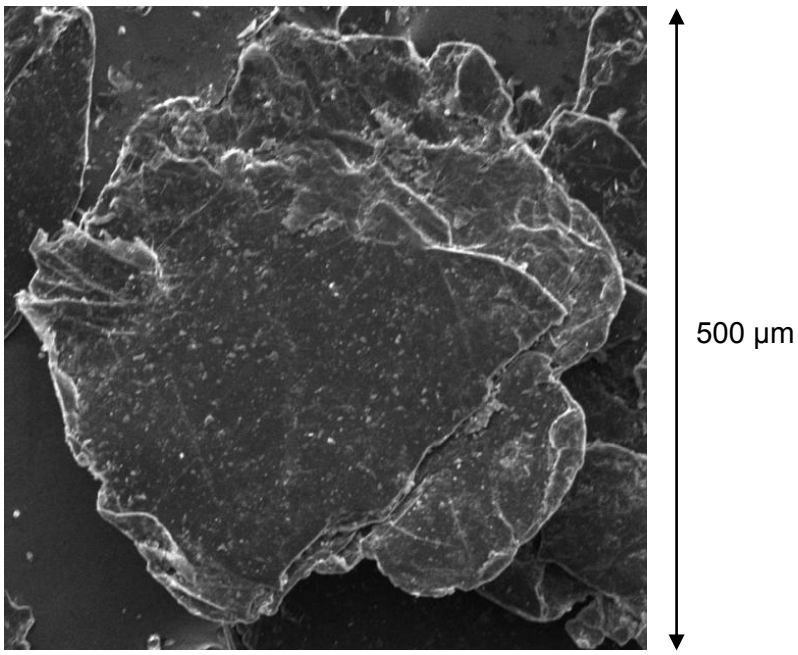

Fig. 17. SEM image indicating the length and width of graphite flakes

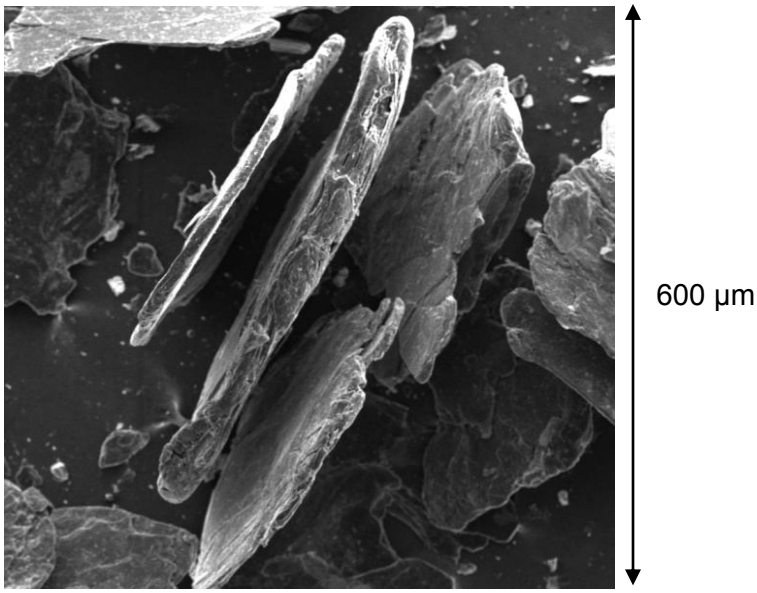

Fig. 18. SEM image indicating the thickness of graphite flakes

As discussed in section 2.3, the average surface roughness of the graphite flakes is required as an input to calculate the TCR between adjoining graphite flakes using the model developed by Bahrami et al [82]. To determine the surface roughness, individual

graphite flakes were inspected using atomic force microscopy (AFM) [83]. AFM is a method of microscopy in which a very sharp probe scans a surface to image and measure surface properties of the sample.

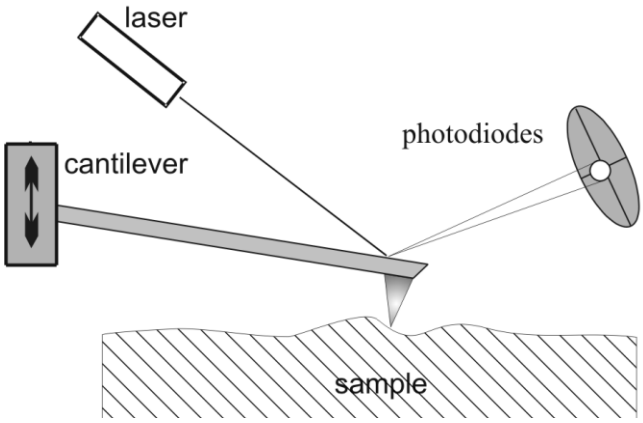

Fig. 19. Schematic and working principle of AFM

There are three main imaging modes in AFM: non-contact mode, intermittent mode, and contact mode [84]. Contact mode is the most common type of AFM microscopy being used, which operates by sweeping a sharp probe which acts as a scanner attached to a cantilever with low spring constant across the sample [85]. The deflection of the probe is recorded and converted into an image of the sample surface [86,87]. Using this technique, the root mean square (RMS) surface roughness can be calculated [88]:

$$\sigma = \sqrt{\frac{1}{L}\int_0^L |Z^2(x)|\, dx} \tag{17}$$

where *Z(x)* is the height (Z) as a function of position (x) of the sample, over the sweeping length "L". The AFM measurements were repeated for 20 graphite flakes and the RMS roughness values were obtained. The average value of the 20 measurements was used as the average surface roughness, σ, in Eq. 13.

Table 7. AFM measurements of flake surface roughness

Flake Number	RMS Surface Roughness (nm)
1	217
2	230
3	235
4	244
5	219
6	234
7	212
8	223
9	250
10	261
11	220
12	218
13	231
14	225
15	224
16	239
17	235
18	219
19	239
20	228
Average	230.15
Standard Deviation	12.30

2.4.4. Numerical modeling

Constriction resistance, which is mainly a geometrical effect, can be defined as the resistance introduced to the heat path when heat has to transfer from a larger cross section area to a smaller one. If the geometry of the self-consistent field consisted of only a strip of pure carbon material, *i.e.*, if a=0, then the flake-level constriction resistance will be zero. The small gap between adjoining flakes introduces a constriction resistance. Since flake aspect ratio (λ) for the graphite flakes used in this study is a large

number (20-25), the temperature distribution is almost one-dimensional in most of the self-consistent field for each of the in-plane and through-plane heat transfer cases.

Constriction resistance can be introduced by a factor ω_x (or ω_y) multiplied by the bulk thermal resistance of the graphite flake. In order to calculate appropriate values for ω, numerical simulations of heat conduction in the unit cell were performed. The self-consistent field was modeled in COMSOL Multiphysics, which contains two adjoining graphite flakes placed on top each other with an offset that resembles the air gap between the flakes. Steady state heat conduction through the graphite flakes with constant thermophysical properties was modeled in the program. As shown in Fig. 20, a constant inward heat flux is assumed to be exerted on the surface of the top graphite flake and a convective heat flux is assumed to affect the lower graphite flake. The sides of the self-consistent field are assumed to have symmetry boundary conditions. The problem is solved for graphite flakes stacked on top of each other with and without offset, and it is observed that the offset will introduce a constriction resistance that increases the bulk thermal resistance of the self-consistent field by 19.5%, thus the constriction factor will be considered ω=1.195. The problem was calculated for fine meshes with more than 5190 grids and coarse meshes with 1440 total number of grids, and the results were consistent. Therefore, it was concluded that the study is grid independent.

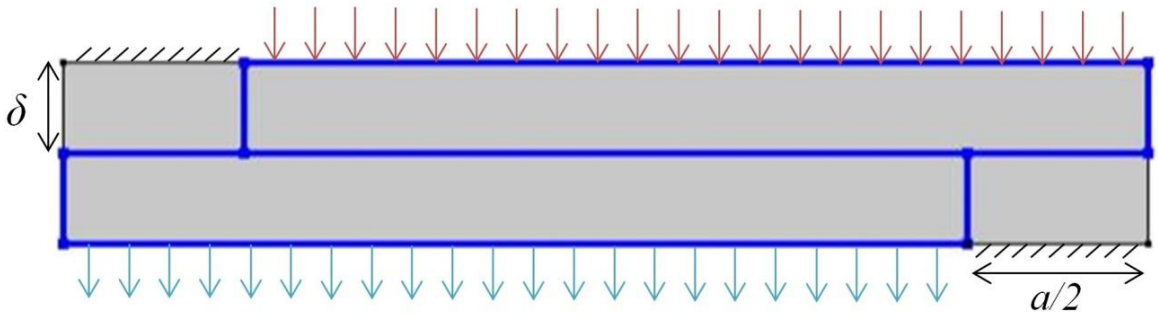

Fig. 20. Boundary condition of graphite flakes

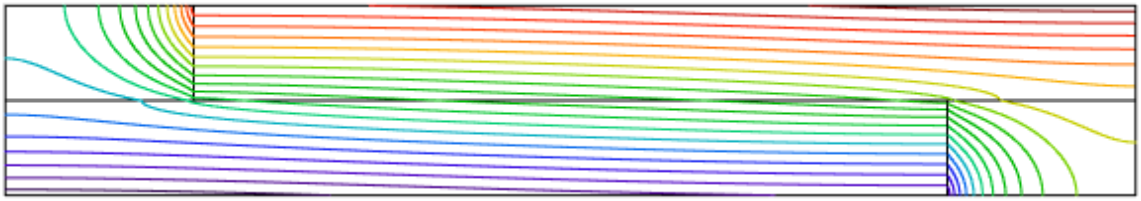

Fig. 21. Results of numerical modeling indicating the isotherms in stacked graphite flakes

2.5. Results and Discussion

In order to investigate the effect of compressive pressure on the thermal conductivity of the graphite sheets, several pre-compressed graphite sheets, manufactured by Terrella Energy Systems, were tested by the guarded heat-flux meter. Graphite sheets with different thicknesses, prepared under 100MPa pressure were tested. Fig. 22 shows the measured thermal resistances of the tested graphite sheets versus compressive pressure. It should be noted that the thermal resistance plotted in Fig. 22 is comprised of two different thermal resistances, which are different in nature: 1- bulk thermal resistance of the graphite sheet and 2- thermal contact resistance between the heat-flux meters and the graphite sheet. As shown in Fig. 22, the total thermal resistance of the graphite sheets decreases with increasing compressive pressure. This is due to the fact that the TCR between the samples and the heat-flux meters is highly dependent on pressure. The difference in thermal resistance of the two graphite sheets is due to the increased bulk thermal resistance, because of the increase in thickness.

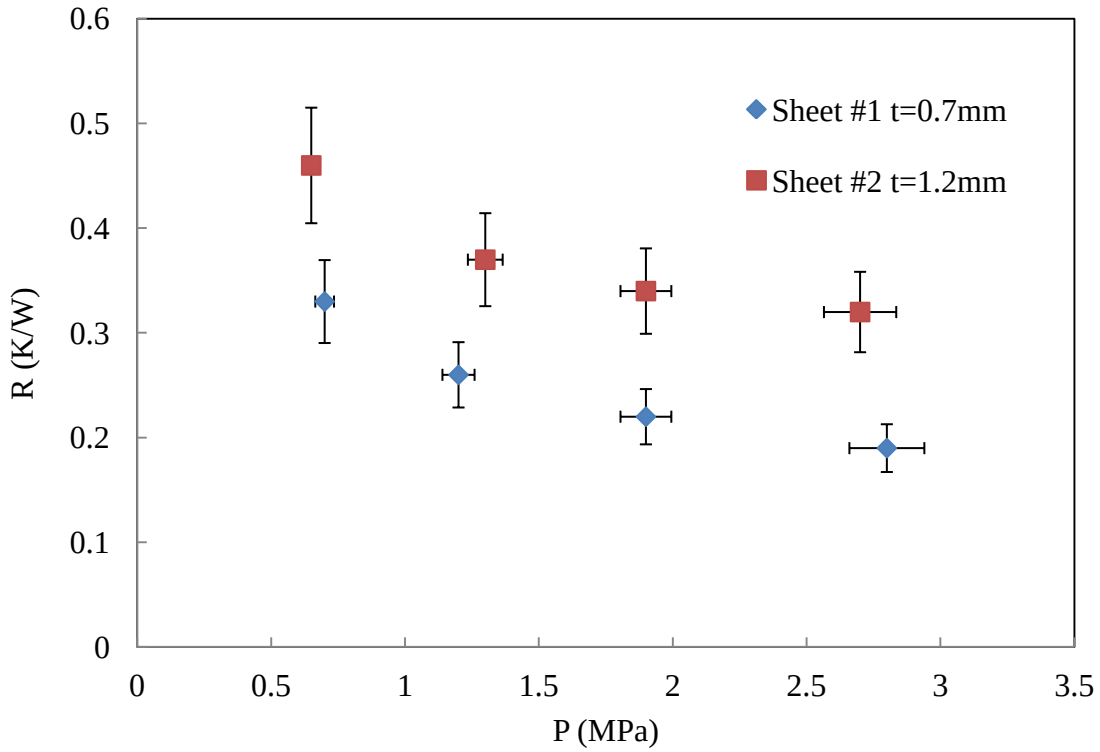

Fig. 22. Through-plane thermal conductivity of the pre-compressed NFG sheets with respect to the compressive pressure

It is inferred from Fig. 22 that the difference in thermal resistances of the sheets remains constant by increasing pressure. This means that the thermal conductivity of the tested graphite sheets is independent of pressure. The reason behind this observation is that these graphite sheets were pre-compressed under excessive compression pressure, which is much higher than the range in which the sheets were tested. To measure thermal conductivity of the compressed NFGs under low compression, NFGs were compressed using the loading mechanism of the guarded heat-flux meter device, described in the experimental study section. The loading sensor is capable of bearing a maximum of 8.6MPa compression; hence, the through-plane thermal conductivity of the compressed NFGs was measured under compression pressures lower than 8.6MPa. Two different thicknesses of the compressed graphite flakes were tested and their through-plane thermal conductivities were measured and reported.

Using the values obtained from SEM imaging, AFM measurements, and the work done by Richter et. al [89], Eq. 13 can now be used to calculate the thermal conductivity of the compressed graphite sheets. Table 8 shows the set of parameters used in the aforementioned equations and their numerical values.

Table 8. Numerical values of the parameters used in the model

Parameter	Value
L	600μm
δ	25μm
a	50μm
ω_y	0.55
σ	230 nm
c_1	10.5E9 Pa [89]
c_2	-0.21 [89]

The geometrical values in this table, such as flake length, *L*, flake thickness, *δ*, and the gap between flakes, *a*, were estimated based on the SEM images of the graphite flakes and surface roughness was measured with AFM. Using the values listed in Table 8, the results of the model for the through-plane thermal conductivity of the graphite sheets are shown in Fig. 23. It should be noted that the model was developed for a simplified structure of the graphite sheet and it was assumed that this structure was repeated uniformly though the structure. However, the measured values for geometrical dimensions of the flakes indicated that there is inconsistency in the thickness of the graphite flakes. If two adjoining graphite flakes have different thicknesses, then the graphite flakes on top of those would be tilted, creating extra gaps along the length of the flakes. These extra gaps can greatly reduce the through-plane thermal conductivity of the graphite sheets, while the model does not account for these imperfections, due to complexity. Therefore, the fitting parameter was introduced to compensate for the over-prediction of through-plane thermal conductivity of the graphite sheets, due to geometrical imperfections.

Fig. 23 shows the effect of the fitting parameter on the analytical model and its accuracy. Changes in the fitting parameter directly affect the slope of the line and can

alter the results. It was observed that ω=0.55 results in the best agreement between the analytical model and experimental results.

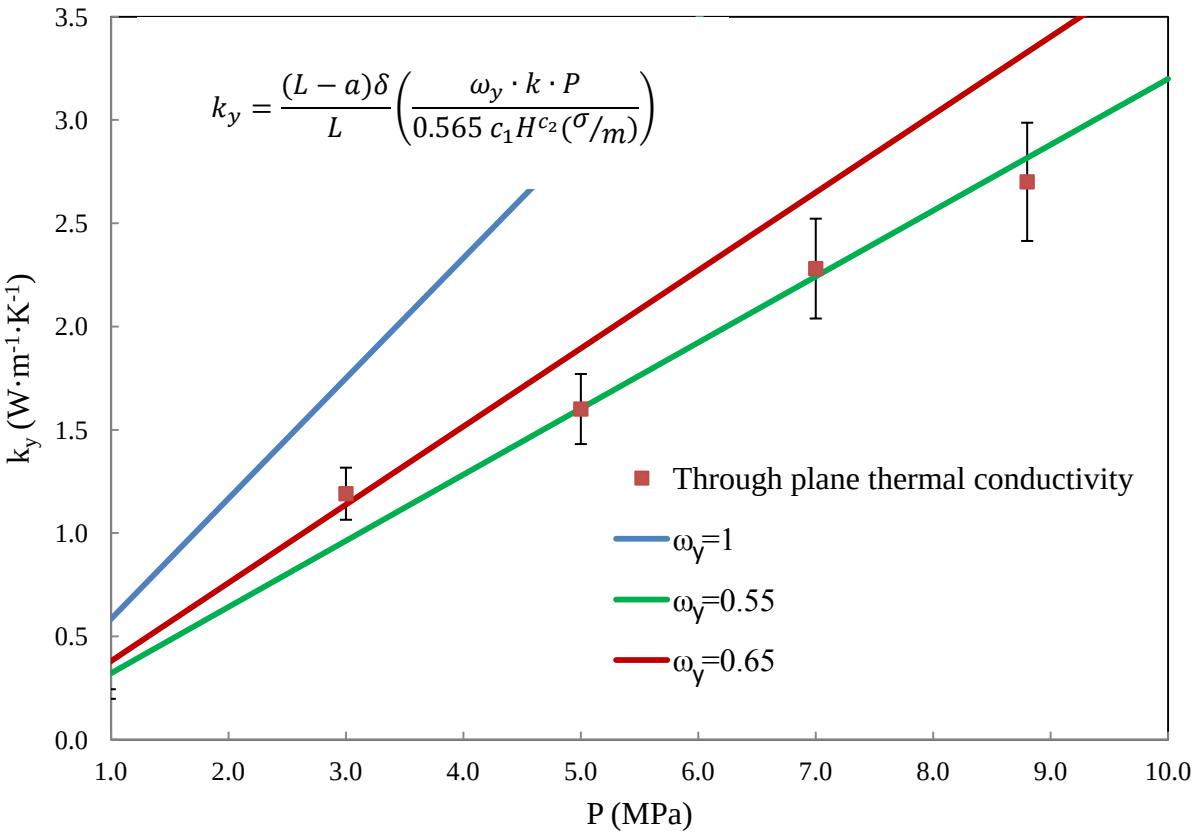

Fig. 23. Through-plane thermal conductivity of the graphite sheets with respect to the compressive pressure

In order to understand the sensitivity of the modeling results to the salient geometrical parameters, the model was used to calculate thermal conductivity of graphite flakes with different geometrical dimensions. Fig. 24 shows the results of the model for graphite flakes with different lengths. It was observed that longer graphite flakes slightly increase the thermal conductivity of graphite sheets. The reason for this trend is that increasing the length of graphite flakes directly increases the area of heat transfer and reduces the thermal resistance of the unit cell, thus increasing the thermal conductivity of the graphite sheet.

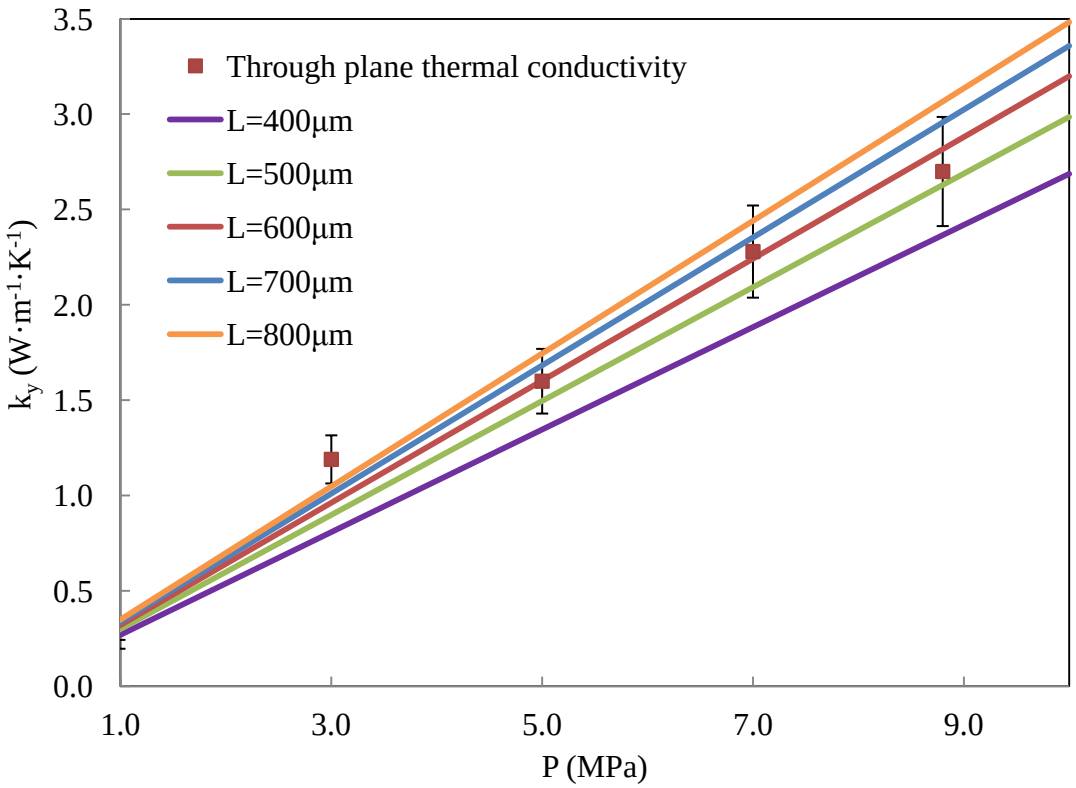

Fig. 24. Thermal conductivity of the graphite flakes with different lengths

A similar sensitivity analysis was done for the thickness of graphite flakes and the results were plotted in Fig. 25. It was observed that graphite sheets manufactured from thicker graphite flakes resulted in higher thermal conductivities. If the thickness of graphite flakes was increased by 25 percent, the through-plane thermal conductivity of the graphite sheet at 5MPa was approximately 30 percent higher. However, increasing the length of graphite flakes by 25 percent led to only 5 percent increase under the same pressure. The reason for this discrepancy is that by increasing the flake thickness, the number of graphite flakes that can be fitted in the unit height of graphite sheets is decreased, which leads to a reduction in the number of TCRs in the through-plane direction. As explained in the modeling section, the main thermal resistance in the unit cell formed by graphite flakes is the TCR. Thus, by decreasing the number of TCRs, the thermal conductivity of graphite sheet is increased.

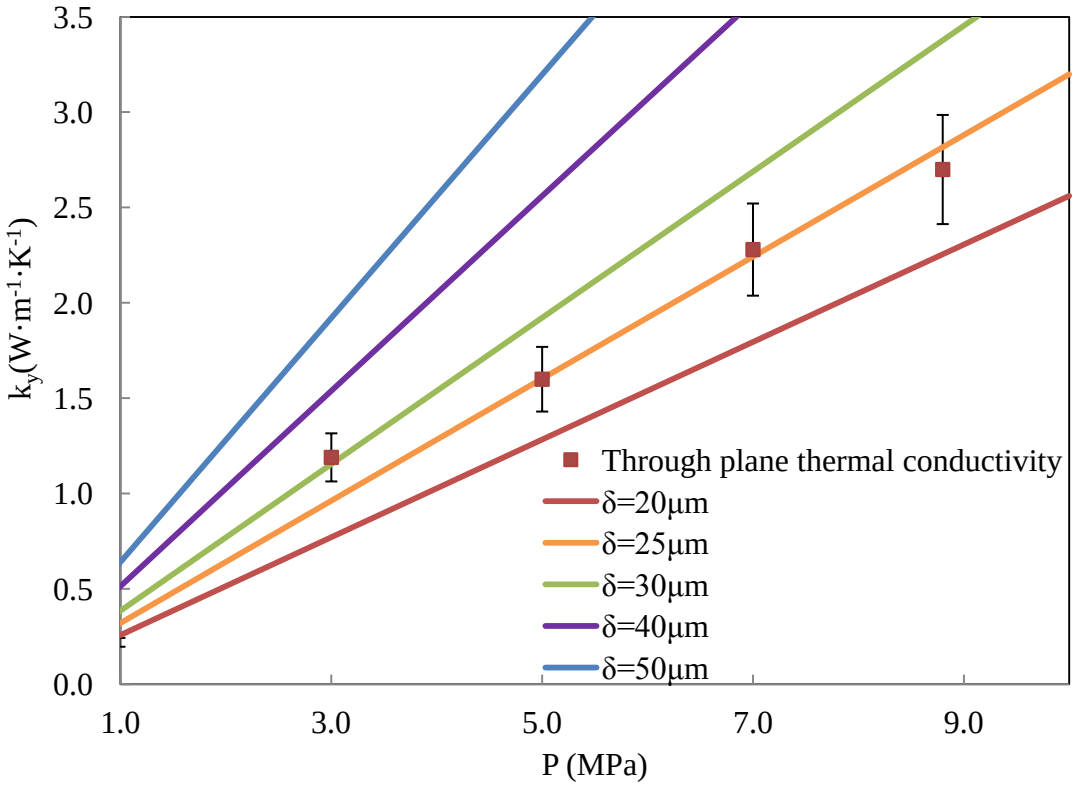

Fig. 25. **Thermal conductivity of the graphite flakes with different thicknesses**

2.6. Conclusion

The effective thermal conductivity of the graphite sheets manufactured by compressing graphite flakes was modeled based on the micro-level geometrical data and the arrangement of the graphite flakes. A block of flexible graphite sheet with dimensions of unity was assumed as a two-dimensional matrix of pure carbon flakes stacked upon each other. The unit cell approach has been incorporated to estimate the thermal resistance of a single representative unit within the structure and the effective thermal conductivity of the graphite sheet was calculated. The thermal contact resistance between graphite flakes was modeled as a function of pressure, which directly affects the thermal conductivity of the graphite sheet. The thermal contact resistance between adjoining flakes was found to be the dominant resistance in the unit

cell, especially at lower pressures. It was shown that through-plane thermal conductivity of the graphite sheet increases by increasing the compression pressure, since higher pressure translates into lower thermal contact resistance between the flakes and in turn more heat conduction through the contact area. The gaps between graphite flakes cause a constriction resistance, which is calculated using numerical analysis. The thermal contact resistance between adjoining flakes were calculated and found to be the dominant resistance in the unit cell especially at lower pressures.

The model was compared to the experimental data and good agreement was observed, with maximum discrepancy of less than 10% between the analytical model and the experimental data. It is noteworthy that the model overestimates the effective thermal conductivity of the graphite sheets at low pressures. The reason is that at low pressures, intimate contact between the graphite flakes is not assured, and there may be significant gaps between the graphite flakes. However, the model is based on the assumption that the flakes are in intimate contact and there is no gap between them.

Chapter 3. Improving Thermal Performance of the Printed Circuit Boards (PCBs) through Using Thermal Vias

3.1. Preface

One of the popular thermal management methods, specifically for highly-populated electrical boards, is to transfer the heat generated in the components to the back-side of the PCB, and then dissipate it to the ambient using heat sinks or other cooling methods. PCBs provide mechanical support and connect components electronically. One of the major challenges facing the current technology of PCB is to remove the dissipated heat from electronic components effectively to prevent failures caused by overheating and thermal stresses. This task can be achieved via attaching a heat sink to the backside of the PCB. PCBs are generally made of several layers of FR4, which is a composite material made of woven fiberglass with epoxy resin binder and has a low thermal conductivity. The low through-plane thermal conductivity of FR4; however, is the main drawback of this cooling method. Thus, for this cooling method, in which the PCB may be the bottleneck for the heat flow, a proper design of the PCB will become essential.

The interconnect network of copper in PCB not only electronically connects the components, but also contributes to the effective thermal conductivity of the PCB. Thus, the effective thermal conductivity of PCB is higher than pure FR4. PCBs are highly anisotropic, due to their layered structure. Thermal conductivity of PCB, in in-plane direction, is higher compared to its through-plane direction; however, the through-plane thermal conductivity of PCB is more crucial for thermal management purposes.

In order to increase the thermal conductivity of PCB, an array of copper plated through holes can be used to transfer heat from one side of PCB to the other. These copper plated through holes are usually referred to as thermal vias. If thermal vias are located on PCB effectively, the through-plane thermal conductivity of the PCB will be greatly increased which can prevent local hot spots formation and increase the circuit life time. On the other hand, adding thermal vias will increase the cost, weight and complexity of the PCB design. As a result, it is important to have an in depth understanding of heat transfer through the thermal vias and their contribution to the effective thermal conductivity of PCB.

3.2. Literature Review

Finding a cost effective method to improve the through-plane heat transfer in PCBs, has been the research focus area of many researchers. Li [90] presented an analytical model by considering a 1-D heat transfer through PCB in form of a network of parallel thermal resistances. Through single and multiple thermal via modeling, an analytical relationship of thermal resistance versus the via design parameters was reported in a dimensionless form. Li also optimized the design parameters of thermal vias by using the thermal resistance as an objective function. Azar and Graebner [91] used infrared microscopy to measure the through-plane thermal conductivity of PCBs with embedded layers of copper. They reported the through-plane thermal conductivity of woven-glass epoxy composite to be 0.29 W/m·K. They also found that the contact between copper and FR4 is sufficiently good that the thermal contact resistance is negligible. McCoy and Zimmermann [92] conducted a feasibility study which proved that the thermal via concept could be implemented for cooling purposes. They also demonstrated that the thermal path will have negligible degradation for a 15-year life equivalent in airborne environment. Monier-Vinard et al. [93] derived a compact analytical model to estimate the temperature distribution in each layer of a multi-layered PCB. Their model could be used to optimize the conductive path from the sensitive thermal surfaces of the package to the PCB. Shabany [94] studied variations of thermal conductivity of PCB with component size using three dimonsional numerical simulations.

It was shown that the effective thermal conductivity of the PCB with copper layer was larger than the values predicted by their 1-D model, if the components mounted on a PCB were smaller than the PCB itself. Asghari and Park [95] studied steady state thermal resistance from a heat source on top of a PCB to the bottom of the board and performed an optimization study on thermal vias and PCB to predict the lowest thermal resistance path directly beneath high power dissipating transistors. Their results indicate that to achieve lower thermal resistances, the thermal via pitch size should be decreased, while the copper barrel thickness should be increased. Yu et al. [96] presented a cost-effective thermal solution using FR4-based PCB and filled and capped thermal vias to enable superior thermal performance on board-level for closely packed power light emitting diodes (LEDs). They found no solder joint or board-level failure during temperature cycling tests for PCB with thermal vias when monitoring changes of board thermal resistance. Kafadarova and Andonova [97] ran thermal simulations with and without thermal vias and found out that the temperature gradients in the through-plane direction were almost two orders of magnitude larger than the in-plane direction. They validated their simulation models with experiments. Shin et al. [98] investigated the variation of thermal resistance by constructing thermal via into LED module consisting of copper clad laminate and found out that the increase of copper in thermal via was the primary parameter for decreasing thermal resistance. Gautam et al. [99] selected five different thermal via patterns for a single power device and studied their thermal performance. Using an experimental apparatus, they identified the best patterns of thermal vias with the highest thermal conductivity.

So far, most of the papers published in this area have modeled parameters, such as thermal resistance or temperature distribution and not thermal conductivity, which is the most important factor for thermal performance of PCB. Thus in this paper, an analytical model for thermal conductivity of PCB is developed to predict the effect of vias diameter, copper barrel thickness, and number of vias on the through-plane thermal conductivity of the PCB.

3.3. Model Development

Detailed knowledge of PCB structure is essential for developing an analytical model that can accurately predict the thermal properties of PCBs that feature thermal vias. In this study, several images were taken from the thermal vias using an optical microscope to measure the thickness of the plated copper and via diameter. Fig. 26 shows an image of a thermal via on the solder-plated PCB. A schematic of a round PCB with thermal vias is shown in Fig. 27.

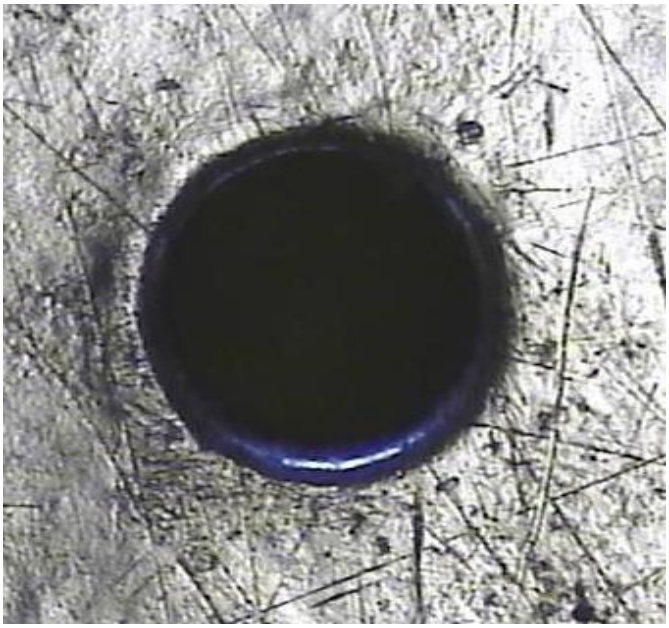

Fig. 26. Thermal via on a copper coated PCB

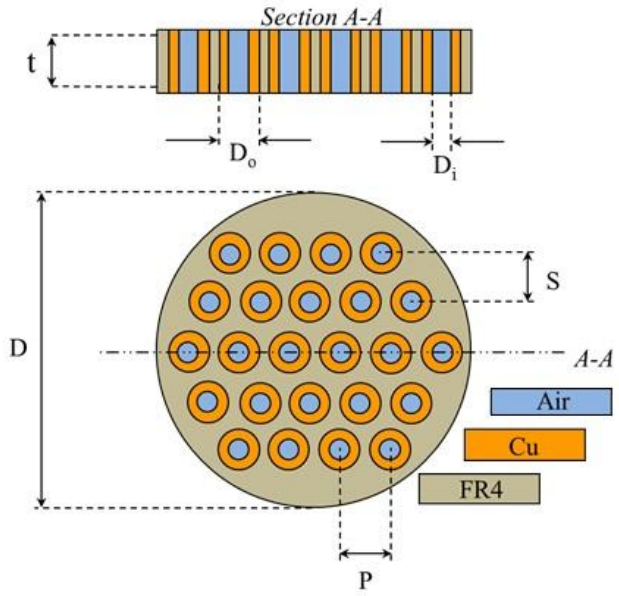

Fig. 27. Schematic of a round PCB with thermal vias

Based on the schematic shown in Fig. 28, two unit cells are defined within the structure for staggered and straight arrangements. It is intuitively evident that the entire structure can be mathematically regenerated by arranging consecutively mirrored copies of the unit cell, and it will be repeated in the entire structure. Thus, a solution of the effective thermal conductivity in the unit cell can be extended to the structure.

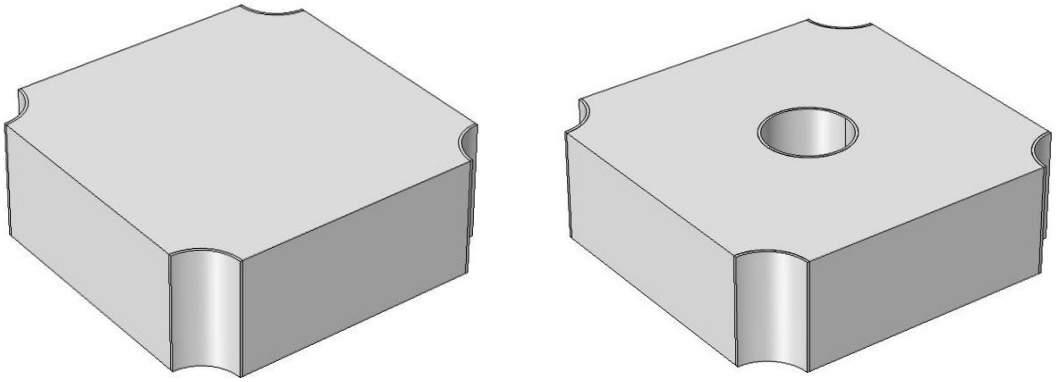

Fig. 28. Schematic of the unit cell, including the thermal vias and the FR4 matrix for square arrangement (left) and staggered arrangement (right)

In general, vias dimensions are usually more than 100 times smaller compared to the dimensions of the PCB itself, and hence it is expected that the properties of the PCB to be closer to the properties of FR4 rather than copper.

Several studies, such as the one by Li [90] have indicated that there was limited heat spreading effect among vias, meaning that the heat either transfers through the copper plating in the vias or through the FR4, and there is minimum heat exchange between the vias and FR4. As such, one dimensional heat transfer analysis was conducted to model the through-plane thermal conductivity of the thermal vias and the FR4 matrix as parallel networks based on the thermal resistance network shown in Fig. 29. Isothermal boundary conditions are applied on the top and bottom surfaces of the PCB.

The total thermal resistance of the PCB with thermal vias can be determined by considering three different components, as shown in Fig. 29.

$$\frac{1}{R_{\text{total}}} = \frac{1}{R_{\text{Cu}}} + \frac{1}{R_{\text{Air}}} + \frac{1}{R_{\text{FR4}}} \tag{17}$$

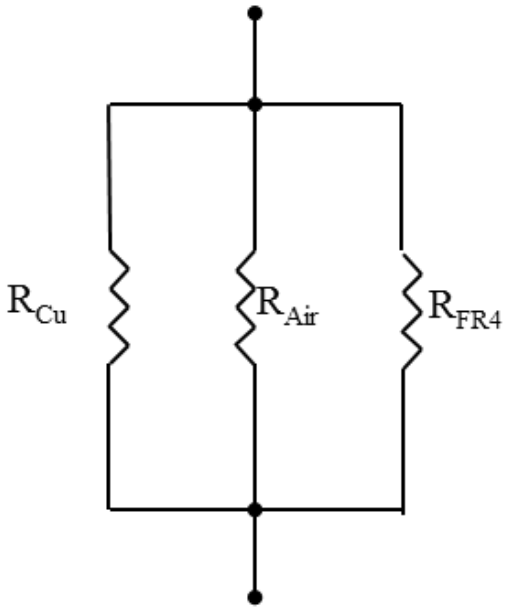

Fig. 29. Network of thermal resistances of individual vias

where R_{total} is the total thermal resistance, R_{Cu} is the thermal resistance of copper, R_{Air} is the thermal resistance of air, and R_{FR4} is the thermal resistance of the FR4 matrix. The thermal resistance of copper is dependent on the thickness of copper barrel plated inside the vias and can be calculated as follows:

$$R_{Cu} = \frac{t}{k_{Cu} \cdot A_{Cu}} \tag{18}$$

where t is the thickness of PCB, *i.e.*, the height of the copper cylinder located inside the thermal via, K_{Cu} is the thermal conductivity of copper, and A_{Cu} is the area occupied by copper in the cross section of the unit cell representing straight and staggered arrangements and can be calculated using following equations:

$$A_{Cu,straight} = \frac{\pi}{4}(D_o^2 - D_i^2) \tag{19}$$

$$A_{Cu,staggered} = \frac{\pi}{2}(D_o^2 - D_i^2) \tag{20}$$

where D_o and D_i are the outer and inner diameters of the copper barrel, respectively. The thermal resistance of air, assuming conduction heat transfer through air, is determined in a similar way to copper:

$$R_{air} = \frac{t}{k_{air} \cdot A_{air}} \tag{21}$$

where k_{Air} is the thermal conductivity of air and A_{Air} is the total surface area of air at the face of PCB and is defined as follows:

$$A_{Air,straight} = \frac{\pi}{4} D_i^2 \tag{22}$$

$$A_{Air,staggered} = \frac{\pi}{2} D_i^2 \tag{23}$$

The thermal resistance of FR4 matrix is:

$$R_{FR4} = \frac{t}{k_{FR4} \cdot A_{FR4}} \tag{24}$$

where k_{FR4} is the thermal conductivity of FR4 matrix and A_{FR4} is the area occupied by this material, which can be calculated as:

$$A_{\mathrm{FR4},straight} = u^2 - \frac{\pi}{4} D_o^2 \tag{25}$$

$$A_{FR4,staggered} = v^2 - \frac{\pi}{2} D_o^2 \tag{26}$$

where *u* and *v* are the sides of the straight and staggered unit cells, respectively. The total thermal resistance of the PCB is defined by:

$$R_{\text{total}} = \frac{T_{s,1} - T_{s,2}}{q_x} = \frac{t}{k_{overall} \cdot A_{total}} \tag{27}$$

By substituting proper terms into Eq. (17) and after some simplifications, the overall thermal conductivity of the PCB with straight and staggered arrangements of thermal vias can be calculated as:

$$k_{\text{overall},straight} = \frac{k_{FR4}\left(u^2 - \frac{\pi}{4} D_o^2\right) + k_{Cu} \cdot \frac{\pi}{4}\left(D_o^2 - D_i^2\right) + k_{air}\frac{\pi}{4} D_i^2}{u^2} \tag{28}$$

$$k_{overall,staggered} = \frac{k_{FR4}\left(v^2 - \frac{\pi}{2} D_o^2\right) + k_{Cu} \cdot \frac{\pi}{2}\left(D_o^2 - D_i^2\right) + k_{air}\frac{\pi}{2} D_i^2}{v^2} \tag{29}$$

As expected, the overall through-plane thermal conductivity of PCB is independent of its thickness and is greatly affected by the inner and outer diameter of the copper.

3.4. Test Samples

Several round PCB samples with different arrangement of thermal vias were prepared for the experimental analysis. The diameter of all the PCB samples were 25.4 mm which was the same as the diameter of the heat flux meters in the guarded heat flux meter test bed, thus the samples could be aligned with the flux meters perfectly.

Four different thermal via arrangements were implanted on the PCB samples with different spacing and pitch values. In order to study the effect of vias' thickness on

the thermal conductivity of PCB, the dimensions of thermal vias embedded in each arrangement were different in some cases.

Table 9 shows the geometrical values of the PCB samples with different thermal vias arrangement used in this study.

Table 9. PCB sample parameters and their ranges

Sample Number	Spacing	Pitch	Via Inner Diameter	Via Outer Diameter	Copper Barrel Thickness
1	2.5	2.5	0.61	0.65	0.04
2	2.5	2.5	0.51	0.55	0.04
3	2.5	2.5	0.36	0.4	0.04
4	2.5	1.25	0.61	0.65	0.04
5	2.5	1.25	0.51	0.55	0.04
6	2.5	1.25	0.36	0.4	0.04
7	1.25	1.25	0.61	0.65	0.04
8	1	1	0.51	0.55	0.04
9	1	1	0.36	0.4	0.04

*All the values reported in the table are in mm.

Several optical microscope images were taken from the cross section of thermal vias to measure their geometrical parameters, such as inner and outer diameter, and copper barrel thickness, as shown in Fig. 30.

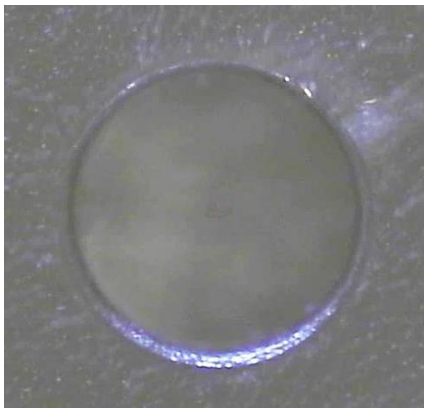

Fig. 30. Cross section of the PCB and the copper plated inside the thermal via

3.5. Numerical Study

As mentioned before, the in-plane heat transfer inside the PCB was neglected in the analytical modeling, and it has been assumed that the FR4 and copper barrels inside the vias will provide parallel paths for heat transfer. In order to verify this assumption, an independent numerical simulation was conducted. The straight and staggered unit cells in Fig. 28 are modeled as a representative geometry. Table 10 shows the major parameters used for the benchmark cases.

Table 10. Parameters used in the benchmark cases

Spacing	Pitch	Via Inner Diameter	Via Outer Diameter	Copper Barrel Thickness	FR4 thermal conductivity	Copper Thermal Conductivity
2.5mm	2.5mm	0.61mm	0.65mm	0.04mm	0.33 W/mK [100]	385 W/mK
2.5mm	1.25mm	0.61mm	0.65mm	0.04mm	0.33 W/mK	385 W/mK

Isothermal boundary condition was assumed for the top and bottom surface of the domain. The top surface was assumed to be at 323K, while the bottom surface was kept at 303K. Due to symmetry, all the sides of the unit cell can be considered insulated. The energy equation was solved using COMSOL Multiphysics. Since there are no specific complexities in the geometry, and also the energy equation was of diffusion type, the problem was expected to be highly grid-independent. Different mesh sizes with total number of grids varying between 12,712 and 94,287 were used and the reported values for total thermal resistance of the PCB, *i.e.*, the ratio of total heat transfer through sample to the temperature different across it, were calculated to be the same up to 4 digits after decimal.

Fig. 31 shows the results of the benchmark case numerical simulations for temperature distribution inside the domain. It should be noted that the boundary conditions are isothermal and the temperature on both sides of the unit cell is constant and uniform. This is the reason why the temperature distribution inside the thermal via is the same as the temperature distribution of FR4. While the temperature distribution is

the same, the heat flux inside the copper is higher than that of FR4 since its thermal conductivity is 1200 times larger.

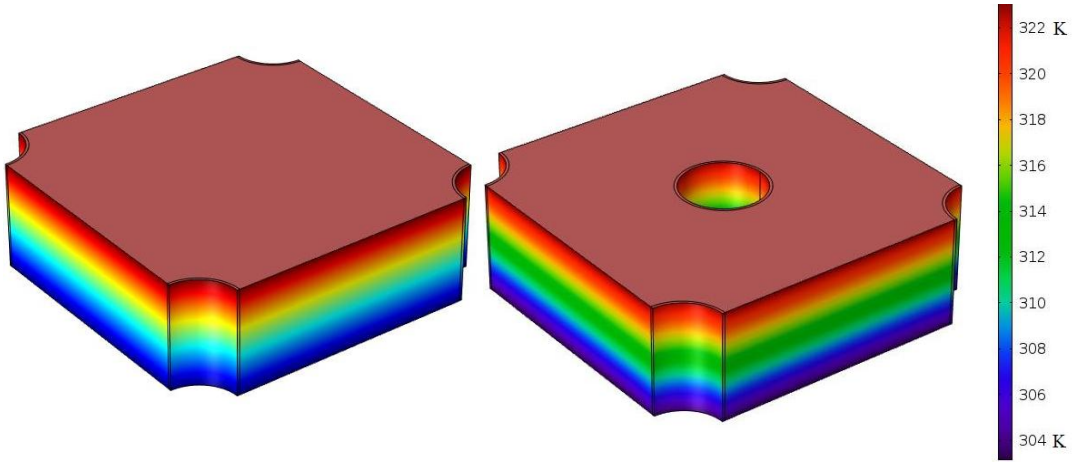

Fig. 31. Temperature distribution in the benchmark unit cell

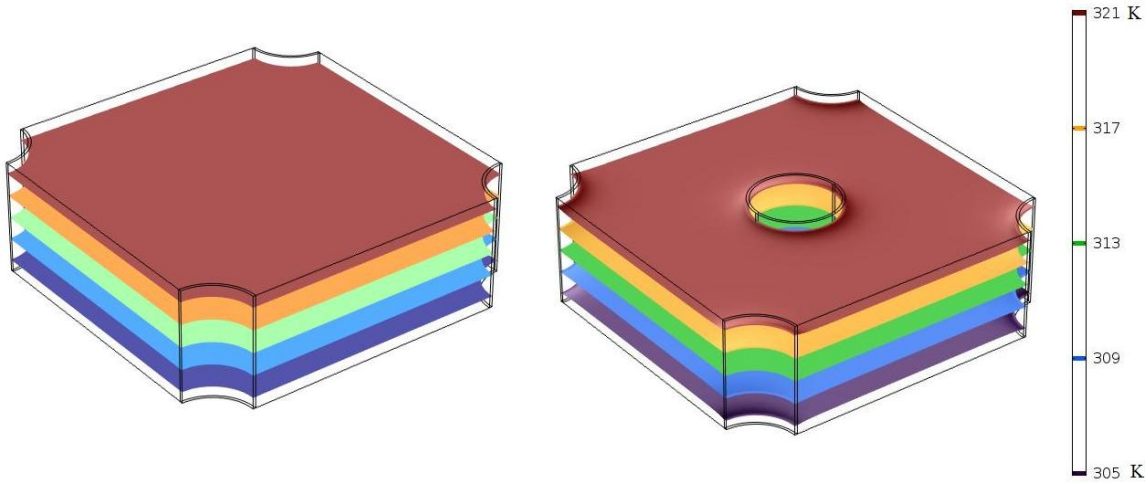

Fig. 32. Isothermal surfaces in the benchmark unit cell

3.6. Results and Discussion

The average values of measured parameters were used in the analytical model, Eq. (25) and Eq. (26), to calculate the effective through-plane thermal conductivity of the PCB with thermal vias for both staggered and straight arrangements. The outcome of the analytical model is shown in Fig. 33 and was compared with experimental, as well as

numerical results. As shown, good agreement between the present analytical model and experimental results was observed, with a maximum relative difference of 13%. The numerically calculated values for thermal conductivity of the PCB were also in close agreement with the analytical model and a maximum discrepancy of 9% was observed.

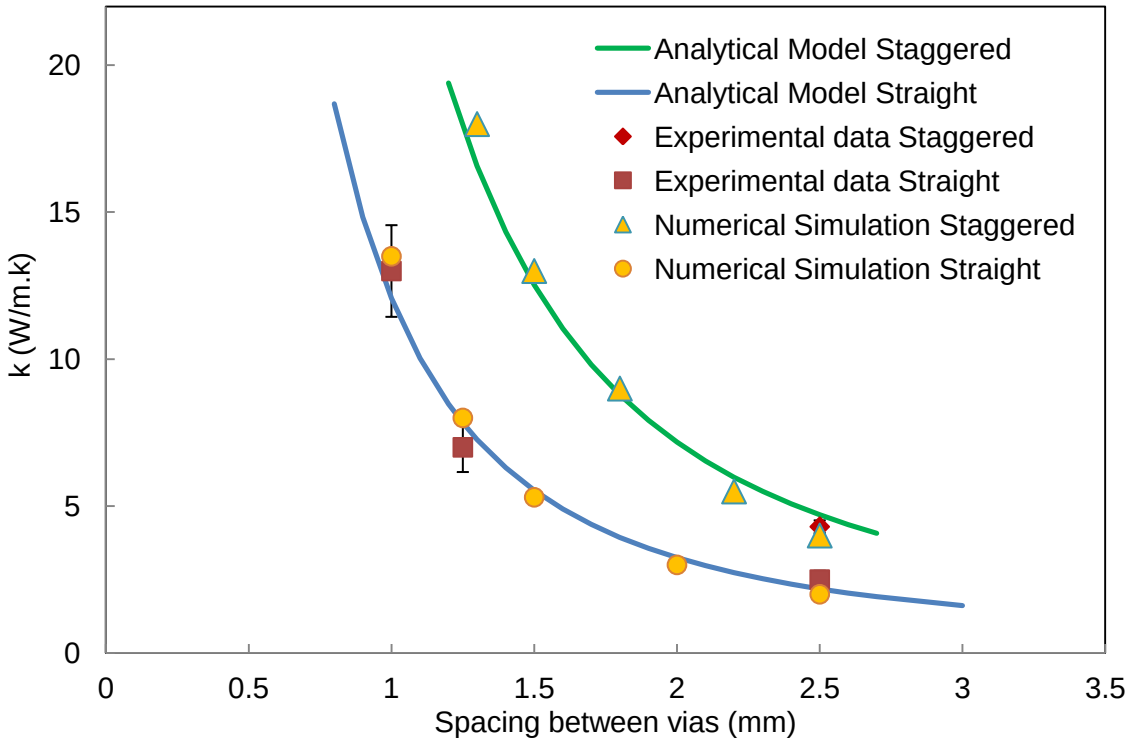

Fig. 33. Thermal conductivity of PCB with two arrangements of thermal vias

As shown in Fig. 33, thermal conductivity of PCB increases as the spacing between the thermal vias is reduced. As previously mentioned, this trend can be explained, since copper acts as a thermal bridge that connects the top and bottom surfaces of the PCB together and reduces its thermal resistance. As the spacing size decreases, the number of thermal vias that can be fitted on a limited space on the PCB increases. Higher number of parallel thermal bridges formed by thermal vias results in better heat transfer through PCB.

Fig. 33 also indicates that the staggered arrangement of thermal vias will result in higher thermal conductivity of PCB than straight arrangement, which is a result of cramming more thermal vias in the available area of PCB.

To understand the effect of each geometrical parameter of thermal vias on the effective thermal conductivity, a parametric study is conducted. Fig. 34 shows the effect of outer diameter of thermal vias on the thermal conductivity of PCB samples which have the same via spacing.

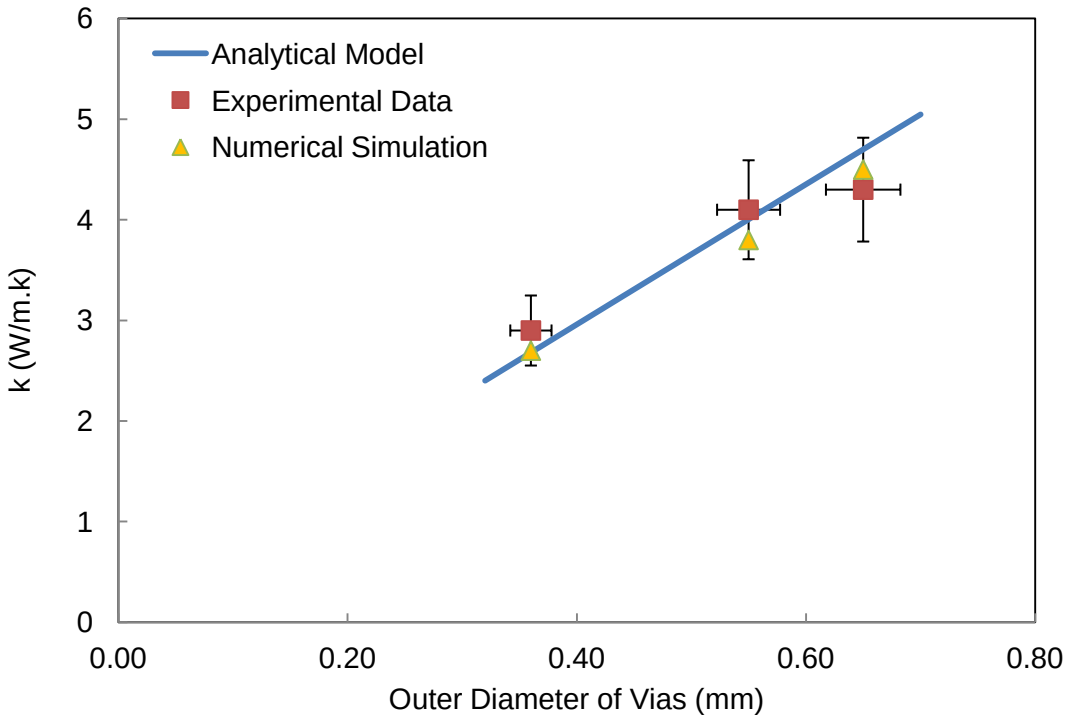

Fig. 34. Effect of outer diameter of thermal vias on thermal conductivity of PCB

It is inferred from Fig. 34 that the effective thermal conductivity of the PCB increases as the outer diameter of thermal vias is increased. These results are plotted for PCBs with staggered arrangement, spacing of 2.5 mm, and different outer diameters. A similar trend is observed for the inner diameter of thermal vias, which is plotted in Fig. 35.

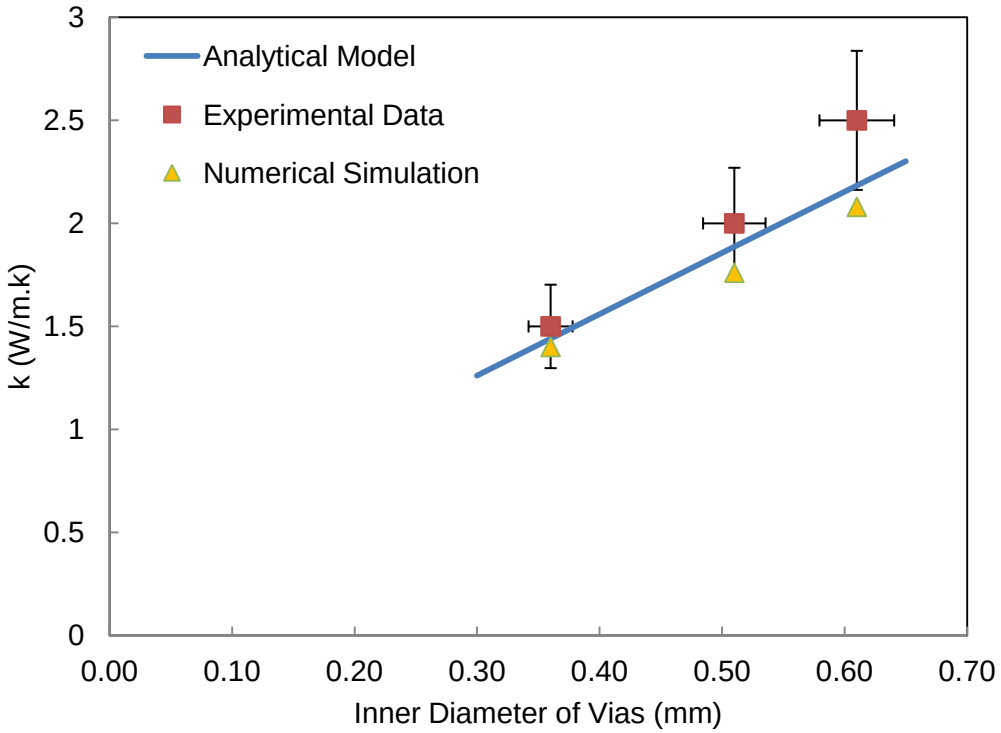

Fig. 35. Effect of inner diameter of thermal vias on thermal conductivity of PCB

It is noteworthy that copper barrel thickness is the same for all of the samples, which means that the difference between inner and outer diameter of plated copper inside the thermal via is constant. Thus, when the inner diameter of the thermal via is increased, its outer diameter increases with the same amount.

3.7. Conclusion

One of the popular thermal management methods is to transfer the heat generated in the components to the back-side of the PCB. In order to achieve this efficiently, thermal vias are designed on the PCB, which act as thermal bridges and increase the thermal conductivity of PCB.

An analytical model was developed based on 1D heat conduction through a network of discrete thermal resistances, in order to predict the effect of vias diameter, copper thickness, spacing, and pitch of vias on the through-plane thermal conductivity of the PCB. Numerical simulation of 1D heat conduction through PCB with thermal vias was done using COMSOL Multiphysics. In order to validate the analytical model, experimental study was conducted to measure the effective through-plane thermal conductivity of PCBs with different via geometrical parameters.

The results indicate that the thermal conductivity of the PCB increases as the area covered by copper is increased. Lower pitch and spacing is desired, since it leads to higher number of thermal vias that can be fitted on a certain available surface area of PCB, which in turn leads to higher thermal conductivity of PCB. It was also concluded that the effective thermal conductivity of the PCB is increased as the outer diameter of thermal vias increases, while keeping its inner diameter constant. In other words, increasing the copper barrel thickness will lead to higher thermal conductivity of PCB.

In the end, the thermal conductivity of different vias arrangements was calculated and the best arrangement of vias on PCB was identified.

Chapter 4. Future Work

The following research directions can be considered as continuation of this study:

- Modeling the anisotropic thermal conductivity of other types of compressed NFG sheets, including resin containing graphite sheets and compressed blended graphite flakes;

- Studying the effect of hysteresis on thermal conductivity of compressed graphite flakes manufactured under different compressing pressures;

- Preparing graphite sheets with different sizes of graphite flakes, running a parametric study on the effect of flake size on effective thermal conductivity of graphite sheets, and using the experimental results in order to validate the sensitivity of the model to flake size;

- Analyzing the possibility of utilizing high thermal conductivity of NFG in thermal vias and increasing the effective thermal conductivity;

- Investigating the effect of thermal vias on electrical performance of electronic chips and studying the trade-offs associated with thermal vias and optimizing their arrangement and size on PCB; and

- Modeling the in-plane heat transfer in PCB with thermal vias, in order to measure the fraction of heat that is being transferred in the plane of PCB.

References

[1] Gurrum, S. P., Suman, S. K., Joshi, Y. K., and Fedorov, A. G., 2004, “Thermal issues in next-generation integrated circuits,” IEEE Trans. Device Mater. Reliab., **4**(4), pp. 709–714.

[2] Anandan, S. S., and Ramalingam, V., 2008, “Thermal management of electronics: A review of literature,” Therm. Sci., **12**(2), pp. 5–25.

[3] Wankhede, M., Khaire, V., Goswami, A., and Mahajan, S. D., 2007, “Evaluation of cooling solutions for outdoor electronics,” Proc. Electron. Packag. Technol. Conf. EPTC, (September), pp. 858–863.

[4] Jahkonen, J., Puolakka, M., and Halonen, L., 2013, “Thermal Management of Outdoor LED Lighting Systems and Streetlights Variation of Ambient Cooling Conditions,” Leukos, **9**(3), pp. 155–176.

[5] Christensen, A., Ha, M., and Graham, S., 2007, “Thermal Management Methods for Compact High Power LED Arrays,” Seventh Int. Conf. Solid State Light., **6669**, pp. Z6690–Z6690.

[6] Nitta, I., Himanen, O., and Mikkola, M., 2008, “Thermal Conductivity and Contact Resistance of Compressed Gas Diffusion Layer of PEM Fuel Cell,” Fuel Cells, **8**(2), pp. 111–119.

[7] Cooper, M. G., Mikic, B. B., and Yovanovich, M. M., 1969, “Thermal contact conductance,” Int. J. Heat Mass Transf., **12**(3), pp. 279–300.

[8] Mikic, B., and Rohsenow, W., 1966, “Thermal contact resistance,” Tech. Rep. DSR 74542-41, (September).

[9] Khandelwal, M., and Mench, M. M., 2006, “Direct measurement of through-plane thermal conductivity and contact resistance in fuel cell materials,” J. Power Sources, **161**(2), pp. 1106–1115.

[10] Zhou, S., Lei, Y., Zou, H., and Liang, M., 2013, “High Thermally Conducting Composites Obtained Via In Situ Exfoliation Process of Expandable Graphite Filled.”

[11] Time, C., and Conductivity, T., 2004, “Measurements on Highly Conductive Alloys (Copper and Copper + Zink Alloy) and commercial PMMA,” (5).

[12] Gwinn, J., and Webb, R., 2003, “Performance and testing of thermal interface materials,” Microelectronics J., **34**(3), pp. 215–222.

[13] Prasher, B. R., 2006, “Thermal Interface Materials : Historical Perspective , Status , and Future Directions,” **94**(8), pp. 1571–1586.

[14] Shahil, K. M. F., and Balandin, A. a., 2012, “Graphene-multilayer graphene nanocomposites as highly efficient thermal interface materials,” Nano Lett., **12**(2), pp. 861–867.

[15] Prasher, R. S., Shipley, J., Prstic, S., Koning, P., and Wang, J., 2003, “Thermal Resistance of Particle Laden Polymeric Thermal Interface Materials,” J. Heat Transfer, **125**(6), p. 1170.

[16] Shin, Y. K., Lee, W. S., Yoo, M. J., and Kim, E. S., 2013, “Effect of BN filler on thermal properties of HDPE matrix composites,” Ceram. Int., **39**(SUPPL.1), pp. S569–S573.

[17] Nabil, M., and Khodadadi, J. M., 2013, “Experimental determination of temperature-dependent thermal conductivity of solid eicosane-based nanostructure-enhanced phase change materials,” Int. J. Heat Mass Transf., **67**, pp. 301–310.

[18] Sharma, A., Tyagi, V. V., Chen, C. R., and Buddhi, D., 2009, “Review on thermal energy storage with phase change materials and applications,” Renew. Sustain. Energy Rev., **13**(2), pp. 318–345.

[19] Kerr, L. L., Pan, Y.-L., Dinwiddie, R. B., Wang, H., and Peterson, R. C., 2009, “Thermal Conductivity of Coated Paper,” Int. J. Thermophys., **30**(2), pp. 572–579.

[20] Viswanath, R., Group, M., and Corp, I., 2000, “Thermal Performance Challenges from Silicon to Systems,” Intel Technol. J. Q3, pp. 1–16.

[21] Mello, K., and Kelley, K., 2001, “An accelerated reliability test method to predict thermal grease pump-out in flip-chip applications,” 2001 Proceedings. 51st Electron. Components Technol. Conf. (Cat. No.01CH37220).

[22] Marotta, E. E., and Fletcher, L. S., 1996, “Thermal contact conductance of selected polymeric materials,” J. Thermophys. Heat Transf., **10**(2), pp. 334–342.

[23] Ino, S., and Shiobara, T., 1994, “Thermal Conductivity Of Molding Compounds For Plastic Packaging,” IEEE Trans. Components Packag. Manuf. Technol. Part A, **17**(4), pp. 527–532.

[24] Lee, G. W., Park, M., Kim, J., Lee, J. I., and Yoon, H. G., 2006, “Enhanced thermal conductivity of polymer composites filled with hybrid filler,” Compos. Part A Appl. Sci. Manuf., **37**(5), pp. 727–734.

[25] Fan, L., and Khodadadi, J. M., 2011, “Thermal conductivity enhancement of phase change materials for thermal energy storage: A review,” Renew. Sustain. Energy Rev., **15**(1), pp. 24–46.

[26] Lyeo, H.-K., Cahill, D. G., Lee, B.-S., Abelson, J. R., Kwon, M.-H., Kim, K.-B., Bishop, S. G., and Cheong, B., 2006, “Thermal conductivity of phase-change material Ge[sub 2]Sb[sub 2]Te[sub 5],” Appl. Phys. Lett., **89**(15), p. 151904.

[27] Prasher, R. S., and Matayabas, J. C., 2004, “Thermal contact resistance of cured gel polymeric thermal interface material,” IEEE Trans. Components Packag. Technol., **27**(4), pp. 702–709.

[28] Balandin, A. A., 2011, “Thermal properties of graphene and nanostructured carbon materials.,” Nat. Mater., **10**(8), p. 569.

[29] Inagaki, M., Kaburagi, Y., and Hishiyama, Y., 2014, “Thermal management material: Graphite,” Adv. Eng. Mater., **16**(5), pp. 494–506.

[30] Gaynes, M. A., and Division, M., “Experimental Determination of the Effect of Printed Circuit Card Conductivity on the Thermal Performance of Surface Mount Electronic Packages.”

[31] Lohan, J., Tiilikka, P., and Rodgers, P., 1999, “Thermal Conductivity on the Operating Temperature of an SO− 8 Package in a Natural Convection Environment: Experimental Measurement versus Numerical,” … Work. Therm. …, (c), pp. 1–7.

[32] Manno, V. P., Kurita, N. R., and Azar, K., 1993, “Experimental characterization of board conduction effects,” IEEE SEMI-THERMm Symp.

[33] Aghazadeh, M., and Mallik, D., 1990, “Thermal Characteristics of Single and Multilayer High Performance PQFP Packages,” **13**(4), pp. 975–979.

[34] Mulgaonker, S., and Chambers, B., 1995, “An Assessment of the Thermal Performance of the PBGA Family,” **18**(4).

[35] Guenin, M., Chowdhury, A. R., Groover, R. L., and Derian, E. J., 1996, “ally Enhanced,” **19**(4), pp. 458–468.

[36] Edwards, D., Hundt, P., and Instruments, T., “Thermal Performance of Tape Based Ball Grid Array Over Molded Packages,” pp. 169–175.

[37] Yovanovich, M. M., “Heat Transfer In Electronic Packaging,” 10th International Heat Transfer Conference, Vol. 1, 1994, pp. 93.

[38] Rodgers, P., 2004, “Prediction of microelectronics thermal behavior in electronic equipment: status, challenges and future requirements,” J. Microelectron. Electron., pp. 1–11.

[39] Rodgers, P., Lohan, J., Eveloy, V., Fager, C.-M., and Rantala, J., 1999, “Numerical, Validating Of Predictions Thermal Component On Interaction Printed Electronic Boards Circuit Forced in Airflows Convection Analysis by Experimental analysi,” Proc. InterPACK’99, (253), pp. 1–12.

[40] Lohan, J., Tiilikka, P., Fager, C.-M., and Rantala, J., 2000, “Effect of both PCB thermal conductivity and nature forced convection environment on component operating temperature: experimental measurement and numerical prediction,” pp. 128–139.

[41] Wissler, M., 2006, “Graphite and carbon powders for electrochemical applications,” J. Power Sources, **156**(2), pp. 142–150.

[42] He, Y., 2005, “Rapid thermal conductivity measurement with a hot disk sensor,” Thermochim. Acta, **436**(1-2), pp. 122–129.

[43] Zhou, S., Xu, J., Yang, Q. H., Chiang, S., Li, B., Du, H., Xu, C., and Kang, F., 2013, “Experiments and modeling of thermal conductivity of flake graphite/polymer composites affected by adding carbon-based nano-fillers,” Carbon N. Y., **57**, pp. 452–459.

[44] Liu, Z., Guo, Q., Shi, J., Zhai, G., and Liu, L., 2007, “Preparation of doped graphite with high thermal conductivity by a liquid mixing process,” Carbon N. Y., **45**, pp. 1914–1916.

[45] Liu, Z., Guo, Q., Shi, J., Zhai, G., and Liu, L., 2008, “Graphite blocks with high thermal conductivity derived from natural graphite flake,” Carbon N. Y., **46**, pp. 414–421.

[46] Yuan, G., Li, X., Dong, Z., Westwood, A., Cui, Z., Cong, Y., Du, H., and Kang, F., 2012, “Graphite blocks with preferred orientation and high thermal conductivity,” Carbon N. Y., **50**(1), pp. 175–182.

[47] Smalc, M., Chen, G., Shives, G., Norley, J., And Iii, R. A. R., 2005, “Interpack 2005-73073 Thermal Performance Of Natural Graphite Heat Spreaders,” Pp. 1–11.

[48] Taira, Y., Kohara, S., and Sueoka, K., 2008, “Performance improvement of stacked graphite sheets for cooling applications,” 2008 58th Electron. Components Technol. Conf., pp. 760–764.

[49] Hermann, A., Chaudhuri, T., and Spagnol, P., 2005, “Bipolar plates for PEM fuel cells: A review,” Int. J. Hydrogen Energy, **30**, pp. 1297–1302.

[50] Mills, A., Farid, M., Selman, J. R., and Al-Hallaj, S., 2006, “Thermal conductivity enhancement of phase change materials using a graphite matrix,” Appl. Therm. Eng., **26**, pp. 1652–1661.

[51] Li, Z., Sun, W. G., Wang, G., and Wu, Z. G., 2014, “Experimental and numerical study on the effective thermal conductivity of paraffin/expanded graphite composite,” Sol. Energy Mater. Sol. Cells, **128**, pp. 447–455.

[52] Zhou, S., Chiang, S., Xu, J., Du, H., Li, B., Xu, C., and Kang, F., 2012, “Modeling the in-plane thermal conductivity of a graphite/polymer composite sheet with a very high content of natural flake graphite,” Carbon N. Y., **50**(14), pp. 5052–5061.

[53] Zhou, S., Xu, J., Yang, Q. H., Chiang, S., Li, B., Du, H., Xu, C., and Kang, F., 2013, “Experiments and modeling of thermal conductivity of flake graphite/polymer composites affected by adding carbon-based nano-fillers,” Carbon N. Y., **57**, pp. 452–459.

[54] Bagheri, F., Fakoor-Pakdaman, M., and Bahrami, M., 2014, “Utilization of orthotropic graphite plates in plate heat exchangers, analytical modeling,” Int. J. Heat Mass Transf., **77**, pp. 301–310.

[55] Zhou, C., Huang, W., Chen, Z., Ji, G., Wang, M. L., Chen, D., and Wang, H. W., 2015, “In-plane thermal enhancement behaviors of Al matrix composites with oriented graphite flake alignment,” Compos. Part B Eng., **70**, pp. 256–262.

[56] Nishino, K., Yamashita, S., and Torii, K., 1995, “Thermal contact conductance under low applied load in a vacuum environment,” Exp. Therm. Fluid Sci., **10**(2), pp. 258–271.

[57] Yovanovich, 2003, “Thermal Spreading and Contact Resistances,” Heat Transf. Handb., p. 133.

[58] Greenwood, J. a., and Williamson, J. B. P., 1966, “Contact of Nominally Flat Surfaces,” Proc. R. Soc. A Math. Phys. Eng. Sci., **295**(1442), pp. 300–319.

[59] Lambert A., M., and Fletcher S., L., 1997, “Review of Models for Thermal Contact Conductance of Metals,” J. Thermophys. Heat Transf., **11**(2), pp. 129–140.

[60] Salerno, L. J., and Kittel, P., 2003, “Measurements of thermal contact conductance,” J. Mater. Process. Technol., **135**(2-3), pp. 204–210.

[61] Liu, G., (Jane) Wang, Q., and Lin, C., 1999, “A Survey of Current Models for

Simulating the Contact between Rough Surfaces," Tribol. Trans., **42**(3), pp. 581–591.

[62] Robbe-Valloire, F., 2001, "Statistical analysis of asperities on a rough surface," Wear, **249**(5-6), pp. 401–408.

[63] Bahrami, M., Culham, J. R., and Yovanovich, M. M., 2004, "Modeling Thermal Contact Resistance: A Scale Analysis Approach," J. Heat Transfer, **126**(December), p. 896.

[64] Zhang, X.-M., and Zhang, X.-X., 2014, "Impact of Compression on Effective Thermal Conductivity and Diffusion Coefficient of Woven Gas Diffusion Layers in Polymer Electrolyte Fuel Cells," Fuel Cells, **14**(2), pp. 303–311.

[65] Karimi, G., Li, X., and Teertstra, P., 2010, "Measurement of through-plane effective thermal conductivity and contact resistance in PEM fuel cell diffusion media," Electrochim. Acta, **55**(5), pp. 1619–1625.

[66] Djilali, N., 2012, "a Statistically Based Thermal Conductivity Model for Pemfc Gas," pp. 1–13.

[67] Sadeghi, E., Djilali, N., and Bahrami, M., 2010, "Effective thermal conductivity and thermal contact resistance of gas diffusion layers in proton exchange membrane fuel cells. Part 2: Hysteresis effect under cyclic compressive load," J. Power Sources, **195**(24), pp. 8104–8109.

[68] Sadeghi, E., Djilali, N., and Bahrami, M., 2011, "Effective thermal conductivity and thermal contact resistance of gas diffusion layers in proton exchange membrane fuel cells. Part 1: Effect of compressive load," J. Power Sources, **196**(1), pp. 246–254.

[69] Sadeghi, E., Bahrami, M., and Djilali, N., 2008, "Analytic determination of the effective thermal conductivity of PEM fuel cell gas diffusion layers," J. Power Sources, **179**(1), pp. 200–208.

[70] Bahrami, M., Yovanovich, M. M., and Culham, J. R., 2006, "Effective thermal conductivity of rough spherical packed beds," Int. J. Heat Mass Transf., **49**(19-20), pp. 3691–3701.

[71] Culham, J. R., and Schneider, G. E., 2006, "Review of Thermal Joint," **59**(January).

[72] Nl, C., 2003, "AIAA 2003-4198 Thermal Contact Resistance of Non- Thermal Model 36th AIAA Thermophysics Conference Meeting and Exhibit."

[73] Bahrami, M., 2004, “Modeling of Thermal Joint Resistance for Sphere-Flat Contacts in a Vacuum.”

[74] Bahrami, M., Culham, J. R., Yovanovich, M. M., and Schneider, G. E., 2004, “Thermal Contact Resistance of Nonconforming Rough Surfaces, Part 1: Contact Mechanics Model,” J. Thermophys. Heat Transf., **18**(2), pp. 209–217.

[75] Analysis, A. S., To, A., and Contact, T., 2003, “IMECE2003-44283.”

[76] Balandin, a. a., Nika, D. L., Ghosh, S., and Pokatilov, E. P., 2009, “Lattice thermal conductivity of graphene flakes: Comparison with bulk graphite,” Appl. Phys. Lett., **94**(2009), pp. 2013–2016.

[77] Nika, D. L., Ghosh, S., Pokatilov, E. P., and Balandin, a. a., 2009, “Lattice thermal conductivity of graphene flakes: Comparison with bulk graphite,” Appl. Phys. Lett., **94**(20), p. 203103.

[78] Fukushima, H., Drzal, L. T., Rook, B. P., and Rich, M. J., 2006, “Thermal conductivity of exfoliated graphite nanocomposites,” J. Therm. Anal. Calorim., **85**(1), pp. 235–238.

[79] Ho, Y. C., Powell, R. W., and Liley, P. E., 1974, “Thermal Conductivity of the Elements: A Comprehensive Review,” J. Phys. Chem. Ref. Data, **3**, p. 810.

[80] Balandin, A. A., Nika, D. L., Ghosh, S., and Pokatilov, E. P., 2009, “Lattice thermal conductivity of graphene flakes: Comparison with bulk graphite,” Appl. Phys. Lett., **94**(20).

[81] Balandin, A. a, Ghosh, S., Bao, W., Calizo, I., Teweldebrhan, D., Miao, F., and Lau, C. N., 2008, “Superior Thermal Conductivity of Single-Layer Graphene 2008,” Nano Lett., **8**, pp. 902–907.

[82] Bahrami, M., Culham, J. R., and Yovanovich, M. M., 2003, “A Scale Analysis Approach to Thermal Contact Resistance,” Heat Transf. Vol. 2, **2003**, pp. 337–348.

[83] Binnig, G., and Quate, C. F., 1986, “Atomic Force Microscope,” Phys. Rev. Lett., **56**(9), pp. 930–933.

[84] Cappella, B., and Kappl, M., 2005, “Force measurements with the atomic force microscope : Technique , interpretation and applications,” **59**, pp. 1–152.

[85] Hutter, J. L., and Bechhoefer, J., 1993, “Calibration of atomic-force microscope tips,” Rev. Sci. Instrum., **64**(7), p. 1868.

[86] Martin, Y., Williams, C. C., and Wickramasinghe, H. K., 1987, “Atomic force microscope-force mapping and profiling on a sub 100-Åscale,” J. Appl. Phys., **61**(10), pp. 4723–4729.

[87] Sader, J. E., Chon, J. W. M., and Mulvaney, P., 1999, “Calibration of rectangular atomic force microscope cantilevers,” Rev. Sci. Instrum., **70**(10), pp. 3967–3969.

[88] Oliveira, R. R. L. De, Albuquerque, D. a. C., Cruz, T. G. S., and Leite, F. M. Y. and F. L., 2012, “Measurement of the Nanoscale Roughness by Atomic Force Microscopy: Basic Principles and Applications,” At. Force Microsc. - Imaging, Meas. Manip. Surfaces At. Scale, p. 256.

[89] Richter, A., Ries, R., Smith, R., Henkel, M., and Wolf, B., 2000, “Nanoindentation of diamond, graphite and fullerene films,” Diam. Relat. Mater., **9**(2), pp. 170–184.

[90] Li, R. S., 1998, “Optimization of thermal via design parameters based on ananalytical thermal resistance model,” ITherm’98. Sixth Intersoc. Conf. Therm. Thermomechanical Phenom. Electron. Syst. (Cat. No.98CH36208), pp. 475–480.

[91] Azar, K., and Graebner, E., 1994, “Experimental Determination,” Society, pp. 1003–1004.

[92] McCoy, B. S., and Zimmermann, M. a., 2004, “Performance evaluation and reliability of thermal vias,” Ninet. Annu. IEEE Appl. Power Electron. Conf. Expo. 2004. APEC ’04., **2**(C), pp. 1250–1256.

[93] Monier-Vinard, E., Laraqi, N., Dia, C.-T., Nguyen, M.-N., and Bissuel, V., 2015, “Analytical modeling of multi-layered Printed Circuit Board dedicated to electronic component thermal characterization,” Solid. State. Electron., **103**, pp. 30–39.

[94] Size, C., Conductivity, E. T., and Boards, P. C., 2002, “Component size and effective thermal conductivity,” pp. 489–494.

[95] Asghari, T. a, and Park, D., 2006, “PCB Thermal Via Optimization using Design of Experiments,” pp. 224–228.

[96] Yu, J. H., Oepts, W., and Konijn, H., 2008, “PC board thermal management of high power LEDs,” Annu. IEEE Semicond. Therm. Meas. Manag. Symp., pp. 63–67.

[97] Kafadarova, N., and Andonova, A., “PCB Thermal Design Improvement Through Thermal Vias 2 CFD Simulations of Conduction Paths,” pp. 241–244.

[98] Hyeong Won Shin, H. S. L., “Analysis on thermal Resistance of LED Modules with vaious Thermal Vias,” pp. 1–4.

[99] Gautam, D., Wager, D., Musavi, F., Edington, M., Eberle, W., and Dunford, W. G., 2013, “A review of thermal management in power converters with thermal vias,” Conf. Proc. - IEEE Appl. Power Electron. Conf. Expo. - APEC, pp. 627–632.

[100] Polanský, R., Prosr, P., and Čermák, M., 2014, “Determination of the thermal endurance of PCB FR4 epoxy laminates via thermal analyses,” Polym. Degrad. Stab., **105**, pp. 107–115.

Appendix

Uncertainty Analysis for Guarded Heat Flux Meter Device

The uncertainty in the measured thermal conductivity of the sample in the guarded heat flux meter device stems from the measured temperature gradient, the cross sectional area, thickness of the sample, spacing of the thermocouples, accuracy of the thermocouples, the thermal conductivity of the flux meters, and the error in extrapolation to calculate the temperature at both ends of the sample.

The temperature gradients in the top and bottom flux meters are always different, since a small fraction of the heat flowing through the flux meters is transferred to the environment through natural convection in the test chamber and radiation. The difference in the measured temperature gradients in the top and bottom flux meters provides an indication of the magnitude of this error. In order to calculate the thermal resistance of the sample, the average of these readings is used, thus the uncertainty could be estimated as half of the difference from the mean. For the experiments conducted in this study, the uncertainty in calculating the temperature gradient for the worst-case scenario would be:

$$\frac{\delta\left(\frac{dT}{dx}\right)}{\left(\frac{dT}{dx}\right)} = \frac{1}{2}\frac{\left(\frac{dT}{dx}\right)_{top} - \left(\frac{dT}{dx}\right)_{bot}}{\left(\frac{dT}{dx}\right)_{ave}} = \pm 0.076 \tag{30}$$

where $\left(\frac{dT}{dx}\right)$ is the temperature distribution in the heat flux meters.

The diameter of the sample is measured using a caliper with the accuracy of ± 0.01 mm. Hence the uncertainty in calculating the cross sectional area of the sample would be:

$$\frac{\delta A}{A} = \frac{2 \times 0.01}{25.4} = \pm 0.0008 \tag{31}$$

where *A* is the cross sectional area of the heat flux meters.

The flux meters were made of a standard electrolyte iron and were calibrated to be within a tolerance of 0.2 W/mK.

$$\frac{\delta k}{k} = \frac{0.2}{73} = \pm 0.003 \tag{32}$$

where *k* is the thermal conductivity of the heat flux meters.

In order to calculate the thermal resistance of the sample, temperature difference across the sample must be known. The accuracy of type *T* standard thermocouples is $\pm 1°\mathrm{C}$, thus:

$$\frac{\delta T_t}{T_t} = \frac{1}{28.3} = \pm 0.035 \tag{33}$$

The temperature at top of the sample is calculated to be 28.3°C by extrapolation. The error of extrapolation is:

$$T_{s,t} = 28.3 \pm 0.15 \tag{34}$$

$$\frac{\delta T_t}{T_t} = \sqrt{(\frac{0.15}{28.3})^2 + (\frac{1}{28.3})^2} = \pm 0.036 \tag{35}$$

Using the same approach, the uncertainty of calculated temperature at bottom of the sample is:

$$\frac{\delta T_b}{T_b} = \pm 0.04 \tag{36}$$

The temperature difference across the sample is calculated by subtracting the extrapolated values for temperatures at both ends of the sample; hence, error propagation should be calculated:

$$\frac{\delta(\Delta T)}{\Delta T} = \sqrt{(\frac{\delta T_b}{T_b})^2 + (\frac{\delta T_t}{T_t})^2} = \pm 0.054 \tag{37}$$

Uncertainty in the calculated value for the total thermal resistance of the sample originates from the aforementioned measurements, which is:

$$\frac{\delta R}{R} = \sqrt{\left(\frac{\delta\left(\frac{dT}{dx}\right)}{\frac{dT}{dx}}\right)^2 + \left(\frac{\delta k}{k}\right)^2 + \left(\frac{\delta(\Delta T)}{\Delta T}\right)^2 + \left(\frac{\delta A}{A}\right)^2} = \pm 0.093 \tag{38}$$

Effective thermal conductivity of the samples was calculated by deducing bulk thermal conductivity and thermal contact resistance from the total thermal resistance. In order to do so, a series of experiments were conducted on samples with same micro-structure and different thicknesses. The thermal conductivity of the samples could be calculated using the following equation:

$$k = \frac{R_2 - R_1}{\Delta t \times A} \tag{39}$$

The thickness of the samples was also measured using a caliper with an accuracy of ± 0.01 mm.

$$\frac{\delta t}{t} = \pm 0.03 \tag{40}$$

Thus,

$$\frac{\delta k}{k} = \sqrt{\left(\frac{\delta t}{t}\right)^2 + \left(\frac{\delta A}{A}\right)^2 + \left(\frac{\delta R_1}{R_1}\right)^2 + \left(\frac{\delta R_2}{R_2}\right)^2} = \pm 0.14 \tag{41}$$

As a result, the maximum uncertainty in calculating thermal conductivity of the samples for the worst-case scenario, occurring at lower compression pressures, was found to be 14%. The uncertainty is decreased at higher compression pressures, due to a significant reduction in the difference between temperature gradients at the flux meters.